Review

Light-emitting molecular devices based on transition metals

Valeria Amendola, Luigi Fabbrizzi *, Francesco Foti, Maurizio Licchelli, Carlo Mangano,
Piersandro Pallavicini, Antonio Poggi, Donatella Sacchi, Angelo Taglietti

Dipartimento di Chimica Generale, Università di Pavia, Chimica Generale, viale Taramelli 12, I-27100 Pavia, Italy

Contents

Abstract

Multicomponent systems have been designed, which are able to perform defined functions related to light emission and quenching. The desired function can be switched ON/OFF by the operator through a chemical input, either a change of pH or a variation of the redox potential. Transition metals (e.g. Ni^{II}, Cu^{II}) are key constituents within the considered systems, playing a distinctive architectural role and favouring electron transfer processes. Investigated devices include *static* molecular switches, in which fluorescence can be quenched/restored through an acid–base or an oxidation–reduction reaction directly involving the metal centre, and *dynamic* switches, in which changes of the light emission intensity follow mechanical motions of the ligating framework. Motions include the oscillation of the pendant arm in scorpionate complexes, the metal ion translocation in a ditopic ligand and the assembling–disassembling of helicates.
© 2005 Elsevier B.V. All rights reserved.

Keywords: Molecular devices; Fluorescence switches; Scorpionates; Helicates; Ion translocation

1. Introduction

Luminescence is a rather rare phenomenon, which refers to the ability of a molecule to emit light, when excited by an incident photon. For instance, excitation may result from the electron transition from a π bonding orbital to a π antibonding orbital (π–π^* excited state) in condensed aromatic hydrocarbons like anthracene, An,

or from an electronic transition from a t_{2g} d orbital of a metal center M to the π antibonding orbital of a ligand L, in an octahedral ML_n complex, like $[Ru^{II}(bpy)_3]^{2+}$ (π_M–π_L^* excited state; bpy: 2,2′-bipyridine). The natural tendency of the excited state to relax to the ground state by releasing a photon of lower energy can be prevented by addressing the excited state to a different process, for instance the transfer of an electron from/to a given reactant Q, displaying donor/acceptor tendencies. In this way, the excited state is deactivated according to a non-radiative way and luminescence is quenched. The process typically

* Corresponding author. Tel.: +39 0382 987328; fax: +39 0382 528544.
  E-mail address: luigi.fabbrizzi@unipv.it (L. Fabbrizzi).

occurs under bimolecular conditions, through the reaction of the excited luminophore with reactant Q. This is the case of anthracene, which, excited by irradiation at 365 nm, in an ethanolic solution, displays its typical emission spectrum with a maximum centered at 400 nm (blue fluorescence observed): on addition of the donor molecule *N,N*-dimethylaniline, DMA, the following electron transfer process takes place: $An^* + DMA \rightarrow An^- + DMA^+$, and anthracene fluorescence is switched off [1]. On the other hand, the complex $[Ru^{II}(bpy)_3]^{2+}$ in aqueous solution, when irradiated at 450 nm, shows yellow-orange luminescence (emission band centered at 627 nm). Luminescence is quenched on addition of the electron acceptor complex $[Fe^{III}(CN)_6]^{3-}$, according to the process: $[Ru^{II}(bpy)_3]^{2+*} + [Fe^{III}(CN)_6]^{3-} \rightarrow [Ru^{III}(bpy)_3]^{3+} + [Fe^{II}(CN)_6]^{4-}$ [2]. The two processes considered above are *inter-molecular* and complete luminescence quenching of either An or $[Ru^{II}(bpy)_3]^{2+}$ requires the addition of a large excess of the donor/acceptor (1000-fold and more), to counterweigh the rather low probability of the reactant Q to collide with the excited luminophore, during its quite short lifetime ($^1An^*$: 6 ns; $^3[Ru^{II}(bpy)_3]^{2+*}$: 627 ns).
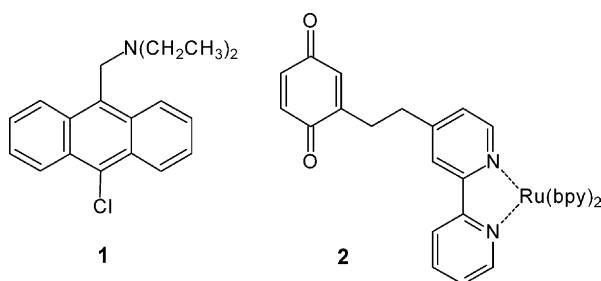
However, it is possible to control the emission of the two considered light-emitting species under *intramolecular* conditions, by appending to their molecular framework an appropriate fragment able to interact with the luminophore. As an example, in system **1**, a tertiary amine group has been linked to the anthracene subunit through a $-CH_2-$ group [3]. At a pH higher than pK_A (=7.7), an electron transfer process takes place from the lone pair of the amine group to the nearby photoexcited anthracene subunit, quenching fluorescence. However, if acid is added to make pH lower than 7.7, fluorescence is fully revived. This happens because, on protonation and formation of the ammonium derivative, the lone pair on the nitrogen atom is no longer available for electron transfer and the excited anthracene fragment can experience its natural radiative decay. Thus, it is possible to turn OFF/ON fluorescence consecutively, at will, through successive additions of standard base and acid, in order to bring pH above/below 7.7. Thus, the amine/ammonium group behaves as a switch, which, operated from the outside through the addition of a given reactant (acid or base), controls the light emission of a connected subunit, anthracene. A further device suitable for luminescence switching is illustrated by formula **2**. In this case, the light-emitting fragment (the bulb, according to

the metaphor from everyday life) is a $[Ru^{II}(bpy)]^{2+}$ subunit, which is covalently linked, through a $-CH_2CH_2-$ spacer, to the control subunit: a quinone moiety, RO_2 [4]. Indeed, RO_2 behaves as a switch of the luminescence of the nearby $[Ru^{II}(bpy)]^{2+}$ fragment. In fact, RO_2, a classical electron acceptor, promotes the occurrence of an electron transfer process from the $[Ru^{II}(bpy)_3]^{2+}$ subunit to itself, thus quenching luminescence. However, on addition of both a reducing agent and strong acid, the quinone fragment is reduced to its hydroquinone counterpart, $RO_2 + 2e^- + 2H^+ \rightarrow R(OH)_2$. Noticeably, as $R(OH)_2$ does not display electron acceptor tendencies, the electron transfer process is suspended and luminescence is restored. Again, light emission by the $[Ru^{II}(bpy)_3]^{2+}$ fragment of system **2** can be switched ON/OFF at command, for instance through a controlled potential electrolysis experiment in aqueous MeCN, by successively adjusting at the pertinent value the potential of a platinum working electrode.

Systems **1** and **2** are classical examples of molecular switches of luminescence, operated by a chemical input. Both systems are *static*, in the sense that switching ON/OFF of the light emission does not involve any nuclear motion, but derives by a mere transfer of electrons [5]. Other molecular devices can be imagined in which luminescence switching is preceded by and is the result of a defined nuclear rearrangement (or molecular motion) [6]. Such switches will be defined *dynamic*.

During the last decade a variety of fluorescence switching devices have been reported [7]. We were particularly interested in the design of fluorescence switches of either static or dynamic nature. As a common prerequisite, all the systems investigated contained transition metal centres and the switching behaviour was expressly related to metal activity. In fact, transition metals display an extremely rich redox activity, a feature of interest in the design of redox switches of luminescence. Moreover, they are very versatile in adopting different coordination geometries, a quality which may induce topological rearrangements and movement of the ligand. This addresses their possible use in the design of dynamic fluorescence switches. The following sections will describe suitable examples of varying classes of luminescent systems, whose emission can be controlled through the activity, either redox or stereochemical, of a transition metal centre.

2. Redox fluorescence switches

The classical paradigm for the design of a redox fluorescence switch involves the covalent linkage of a redox active subunit C and a fluorogenic fragment Fl [8]. Subunit C must exist in two different oxidation states of comparable stability, C_{ox} and C_{red}, and each state should affect the fluorophore and modify its emission to a substantially different extent. C_{ox} and C_{red} are connected through a reversible redox change, and behave in such a way that C_{ox} quenches the nearby fluorophore Fl while C_{red} does not. This situation
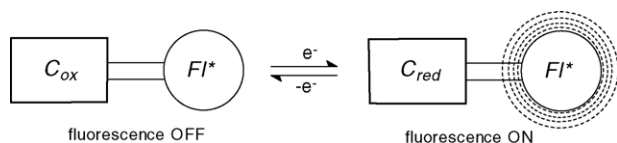
Fig. 1. The covalent linking approach to the design of a fluorescence redox switch. Switch efficiency requires that the redox subunit C in its oxidised form, C_{ox}, quenches the nearby photoexcited fluorophore Fl^* and the reduced form C_{red} does not (OFF/ON switch). The other switching situation (ON/OFF) can be achieved when C_{red} quenches Fl^* and C_{ox} does not. Adapted from Ref. [8].

is pictorially illustrated in Fig. 1. Thus, it is possible to switch light emission ON/OFF at will through the C_{ox}/C_{red} couple, by the successive addition of a reducing agent and an oxidising agent (chemical input) or by alternating the potential of the working electrode in an electrolysis experiment (electrochemical input).

Fig. 2 illustrates the mode of interaction of the control unit C with the proximate excited fluorophore Fl^*, within the covalently linked system $C \sim Fl$. ON/OFF activity arises when one of the two forms of the redox couple, either C_{ox} or C_{red}, quenches the excited fluorophore Fl^* and the other does not. The interaction mechanism between C and Fl^* can be an electron transfer process (eT) or an energy transfer process (ET). The four possible interaction modes are illustrated by the triangular schemes in Fig. 2. Only two combinations generate switching situations: OFF/ON and ON/OFF. In particular, the switch shown in Fig. 1 corresponds to the upper left scheme, OFF/ON.
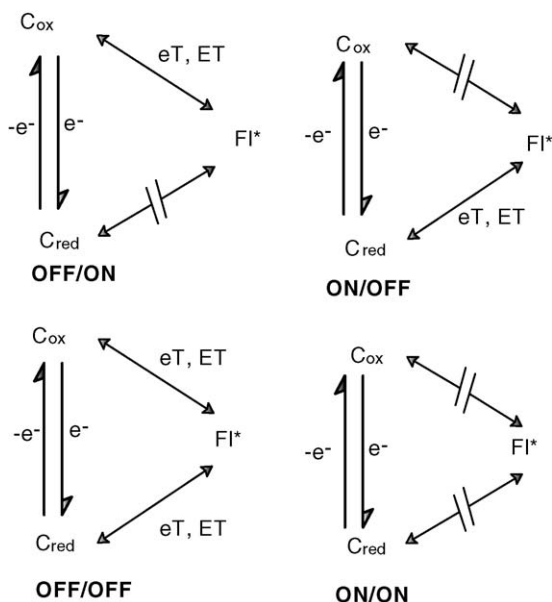

Fig. 2. The basis of redox fluorescence switching in a conjugate system $C \sim Fl$. Either an energy transfer (ET) or an electron transfer (eT) mechanism involving the redox active fragment C can be responsible for the quenching of the covalently linked photoexcited fragment Fl^*. In particular, the switching situation OFF/ON, upper left corner, pertains to the system shown in Fig. 1. Reproduced from Ref. [13], with permission of the copyright owners.

There exist at least three reasons for which it is convenient to use redox active subunits containing transition metal centres: (i) transition metals undergo fast and kinetically uncomplicated one-electron redox changes; (ii) the potential of the redox couple, and the relative stability of the oxidised and reduced form, C_{ox} and C_{red}, can be modulated by varying the nature of the hosting coordinative environment; (iii) transition metals tend to participate in luminescence quenching processes through both eT and ET mechanisms.

Our approach consisted in taking a definite coordinating framework capable of hosting the chosen metal centred redox couple and linking it to a given fluorogenic fragment. A convenient host is represented by the 14-membered tetramine macrocycle cyclam (**3**).
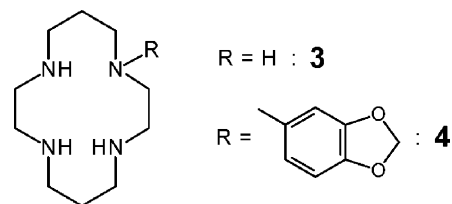
Among polyamine macrocycles of varying denticity and ring size, cyclam and its transition metal complexes exhibit unique properties, which derive from the ligand's ability to situate its amine nitrogen atoms in the positions preferred by most transition metal centres (i.e. the corners of a square) and to establish especially strong coordinative interactions [9]. In particular, (i) cyclam complexes are very resistant to metal extrusion (as an example, $[Ni^{II}(cyclam)]^{2+}$, in spite of the high basicity of the uncoordinated tetramine, lasts in 1 M $HClO_4$ with a half-time of 30 years) [10]; (ii) they can attain unusually high oxidation states of the encircled metal (e.g. Ni^{III}, Cu^{III}, Ag^{II} and Ag^{III}) [11]: this latter property is strictly related to the capability of cyclam to establish strong in-plane interactions, which raise the energy of the HOMO antibonding orbital, essentially metallic in character, from which the electron is abstracted on oxidation. For instance, the potential of the $[Ni^{III}(cyclam)]^{3+}/[Ni^{II}(cyclam)]^{2+}$ couple in 1 M HCl is 0.71 V versus NHE, slightly less positive than that observed for the well-known $[Fe^{III}(H_2O)_6]^{3+}/[Fe^{II}(H_2O)_6]^{2+}$ couple (0.77 V versus NHE) [12], indicating that the Ni^{II} and the Ni^{III} complex have a comparable stability, and are both fairly stable in water. Thus, we considered, for switching purposes, the Ni^{III}/Ni^{II} redox couple, to be hosted within the cyclam ring. Then, we chose as a fluorophore the robust fluorogenic fragment 1,3-benzodioxole, which was linked to one nitrogen atom of the cyclam skeleton through a methylene group. to give **4** [13]. The fluorophore, in an MeCN solution, when excited at 284 nm, shows an intense emission band at 315 nm, with a quantum yield $\Phi = 0.31$. Very interestingly, the Ni^{II} complex of the cyclam–benzodioxole conjugate **4** displays a similar photophysical behaviour: on excitation at 286 nm, an emission bands develops, centred at 326 nm, with a quantum yield $\Phi = 0.21$, indicating that the divalent metal center does not seriously interfere with the
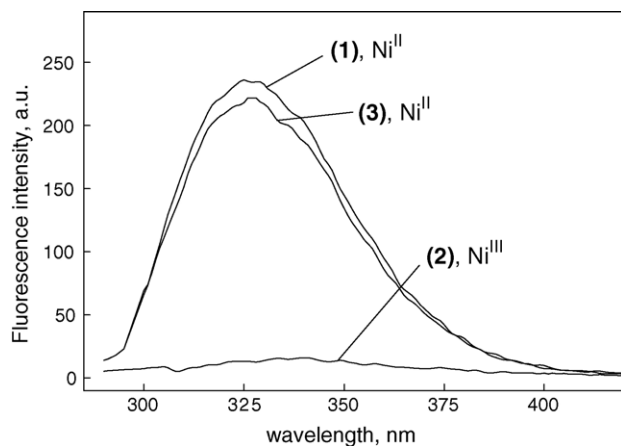
Fig. 3. Emission spectra of an aqueous solution of $[Ni^{II}(4)]^{2+}$ in 0.1 M $HClO_4$, measured during controlled potential coulometry experiments: prior to electrolysis (1, quantum yield $\Phi = 0.20$); after electrolysis at 1.2 V (2, $\Phi = 0.008$); after electrolysis at 0.7 V (3, $\Phi = 0.195$). λ_{exc}: 286 nm. Adapted from Ref. [13].

Fig. 4. Cyclic variation of I_F (fluorescence intensity, arbitrary units) upon consecutive oxidation/reduction processes on the $[Ni^{II}(4)]^{2+}$ complex in aqueous 0.1 M $HClO_4$. Reproduced from Ref. [13], with permission of the copyright owners.

nearby fluorogenic fragment. Cyclic voltammetry studies on an aqueous solution, containing 0.1 M $HClO_4$, indicated a one-electron reversible oxidation process to the Ni^{III} form, with $E_{1/2} = 0.94$ V versus SCE. The switching behaviour was tested by controlled potential electrolysis carried out on a solution of $[Ni^{II}(4)]^{2+}$, in 0.1 M $HClO_4$ as a background electrolyte. Fig. 3 shows the emission spectrum of the solution prior to the electrolysis, pertinent to the $[Ni^{II}(4)]^{2+}$ complex (spectrum (1)): fluorescence is on.

The potential of the working electrode (a platinum gauze) was then adjusted 1.2 V versus SCE (i.e. about 250 mV more positive than the $E_{1/2}$ value determined by CV), in order to perform exhaustive oxidation to Ni^{III}. The emission spectrum of the solution, measured at the end of the electrolysis experiment (after the passage of 1.04 ± 0.05 moles of electrons per mole of complex), showed a drastic decrease of the emission intensity ($\Phi = 0.008$, see spectrum (2) in Fig. 3): fluorescence was off.

On the other hand, on reduction of Ni^{III} to Ni^{II}, performed by adjusting the potential of the working electrode to 0.7 V (i.e. a value ca. 250 mV less positive than the $E_{1/2}$ value), the fluorescence of the solution was progressively restored: in particular, full emission ($\Phi = 0.195$, see spectrum (3) in Fig. 3) was observed after the uptake of 1.05 ± 0.05 moles of electrons per mole of complex: fluorescence was again on. Afterwards, five complete redox cycles could be carried out without any apparent degradation of the $[Ni^{II/III}(4)]^{2+/3+}$ system: in particular, ca. 100% of the fluorescence intensity was recovered after each reduction step (see Fig. 4). Further cycling led to the progressive degradation of the complex, due to the non-perfectly reversible redox exchange.

Fluorescence quenching in the oxidised form of the conjugate system, $[Ni^{III}(4)]^{3+}$, has to be ascribed to an electron transfer process from the excited fluorophore Fl^* to Ni^{III}. The occurrence of such a process can be accounted for on a thermodynamic basis. In particular, the free energy change ΔG_{eT}°,
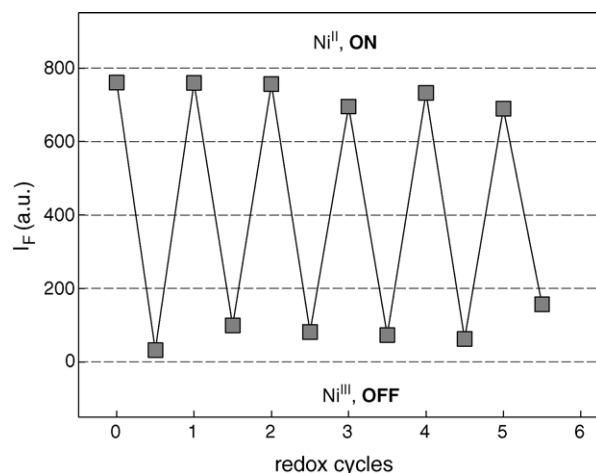
associated with the electron transfer process can be calculated through the thermodynamic cycle illustrated in Fig. 5, by combining the pertinent photophysical and electrochemical quantities: E^{0-0}, the photonic energy, which is obtained from the highest energy band of the emission spectrum, $E^0(Ni^{III}/Ni^{II})$ and $E^0(Fl^+/Fl)$, which refer to the standard electrode potentials for the redox change involving the macrocyclic complex and for the fluorogenic substituent Fl, and can be obtained from the corresponding $E_{1/2}$ values determined in cyclic voltammetry experiments. The calculated ΔG_{eT}° value is distinctly negative (-3.0 eV), and accounts for the quenching of fluorescence occurring in the Ni^{III} derivatives.

A similar thermodynamic approach can also explain why no fluorescence quenching is observed when the system is in the reduced state, $[Ni^{II}(4)]^{2+}$. In fact, the possible eT process (from Ni^{II} to the excited fluorophore), is characterised by a
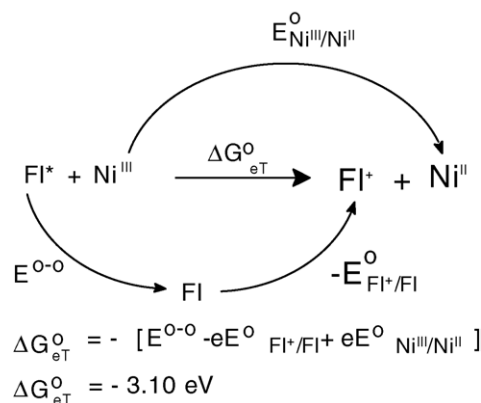

Fig. 5. Thermodynamic cycle for evaluating the free energy change ΔG_{eT}° associated with the intramolecular photoinduced electron transfer in the nickel(III) complex of **4**. $E^{0-0} = 3.80$ eV; $E^0(Fl^+/Fl) = 1.45$ V (irreversible peak); $E^0(Ni^{III}/Ni^{II}) = 0.75$ V. The coulombic term was considered negligible under the present circumstances. Reproduced from Ref. [13], with permission of the copyright owners.
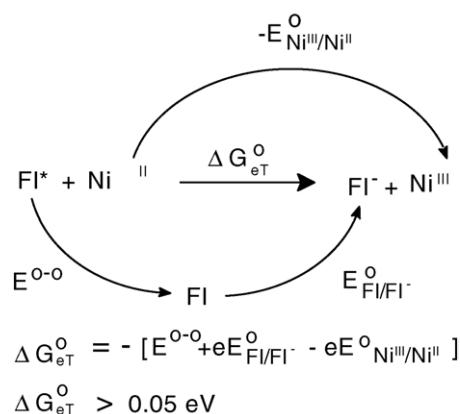
Fig. 6. Thermodynamic cycle for evaluating the free energy change ΔG°_{eT} associated with the intramolecular photoinduced electron transfer in the $[Ni^{II}(\mathbf{4})]^{2+}$. $E^{0-0} = 3.80$ eV; $E^0(Fl/Fl^-) \leq -3.10$ V, since no peaks were observed in the cathodic scan in voltammetry experiments until solvent discharge; $E^0(Ni^{III}/Ni^{II}) = 0.75$ V. The coulombic term was considered negligible under the present circumstances.

positive value of ΔG°_{eT} (≥ 0.05 eV), as calculated from the thermodynamic cycle shown in Fig. 6. The mechanism of the fluorescence switching process for the $[Ni^{II/III}(\mathbf{4})]^{2+/3+}$ redox system, is pictorially illustrated in Fig. 7.

It has been shown in Fig. 2 how the covalent linking of a redox active subunit C, capable of existing in two forms, C_{ox} and C_{red}, reversibly connected through a one-electron change, to a fluorogenic fragment Fl can generate four situations, of which only two provide switching of fluorescence, either OFF/ON or ON/OFF (see Fig. 2). In principle, at least when the quenching process is due to an electron transfer mechanism, one should be able to build an operating switch by choosing appropriate fluorogenic and redox active fragments, whose photophysical and electrochemical properties fit the thermodynamic requirements outlined in Figs. 5 and 6.

In reality, the design of an efficient metal centred redox fluorescence switch is often a matter of chance and the thermodynamic analysis of its functional behaviour is only an elegant a posteriori exercise. Fig. 8 reports a list of systems produced in our laboratory during the last decade.

Most of the switches operate through the OFF/ON mode (C_{ox} quenches Fl^* and C_{red} does not) and are based on two redox couples: Ni^{III}/Ni^{II} and Cu^{II}/Cu^{I}. In some cases, the

mechanism responsible for the OFF state is electron transfer (eT), in others energy transfer (ET). For honesty sake, also some failed projects have been mentioned (systems **8** and **11**), in which both C_{ox} and C_{red} quench Fl^*, giving rise to the unpleasant OFF/OFF situation.

Each redox couple requires its own coordinative environment. It was anticipated that the tetramine cyclam is suitable for the formation of stable complexes with divalent transition metal ions, e.g. Ni^{II}, and also favours the attainment of unusually high oxidation states, e.g. Ni^{III}. The beneficial consequence is that both Ni^{II} and Ni^{III} cyclam complexes display comparable stability in solution, which allows for extended switching from one state to the other, without decomposition. In particular, OFF/ON switches **6** and **7** operate through the Ni^{III}/Ni^{II} redox couple, hosted by a cyclam-like framework [14]. On the other hand, the tetramine cyclam environment is not suitable for the Cu^{II}/Cu^{I} couple. In fact, such a coordinative arrangement stabilises the Cu^{II} state too much compared with Cu^{I}. In particular, the Cu^{I} centre, when obtained through electrochemical reduction of the Cu^{II} tetramine complex, disproportionates to give Cu^{II} and copper metal. Stabilisation of the Cu^{I} state requires a ligand capable of accepting electrons from the metal according to a π mode: this is the case of the thioethereal sulphur atoms present in the macrocyclic receptors of systems **5**, **9** and **10** [15]. In particular, these atoms offer empty $3d_\pi$ orbitals of suitable energy, which overlap with filled $3d_\pi$ orbitals of the metal. As with the Ni^{III}/Ni^{II} systems, the Cu^{II}/Cu^{I} couple leads to OFF/ON switches: the oxidised form quenches the nearby fluorophore while the reduced form does not.

In the list in Fig. 8, there is only one switch operating according to the ON/OFF switching mode (the oxidised form does not quench fluorescence, the reduced form does): it is system **12**, formally based on the Ni^{2+}/Ni^+ redox couple [16]. However, the Ni^+ state does not pertain to an authentic Ni^I metal centre, but to a complex of Ni^{II} with an anion radical ligand: $[Ni^{II}(L^{\bullet-})]^+$. In other words, on reduction of the Ni^{II} complex, the electron from the reducing agent, either a chemical or a platinum anode, does not go to an orbital centred on the metal, but to a π^* orbital of the diene macrocycle. In any case, the $[Ni^{II}(L^{\bullet-})]^+$ complex is able to transfer an electron to the close by excited naphthalene fragment, quenching its fluorescence.
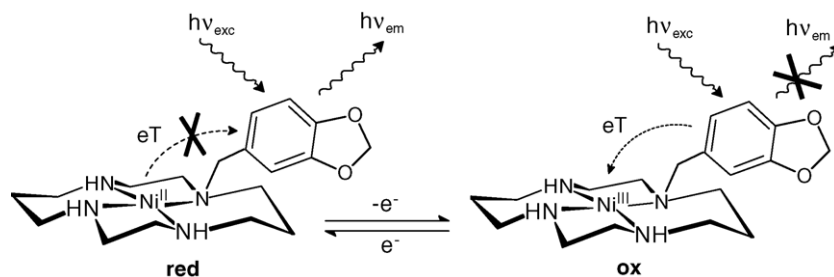

Fig. 7. The mechanism of redox fluorescence switching in the conjugate system $[Ni^{II/III}(\mathbf{4})]^{2+/3+}$: in the oxidised form, **ox**, a fluorophore-to-Ni^{III} electron transfer process takes place and causes fluorescence quenching; in the reduced form, **red**, the Ni^{II}-to-fluorophore electron transfer process is thermodynamically disfavoured and does not take place. On oxidation, fluorescence is quenched, on reduction, is revived.
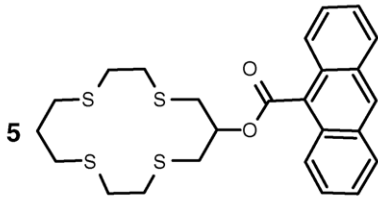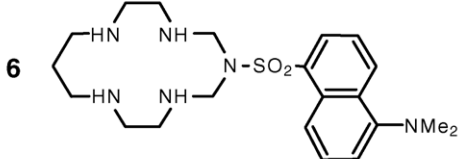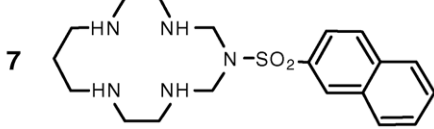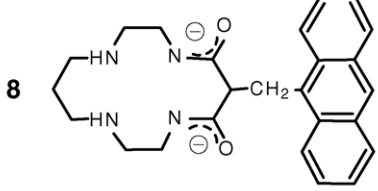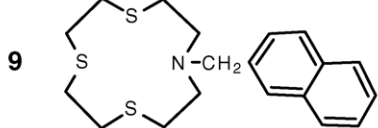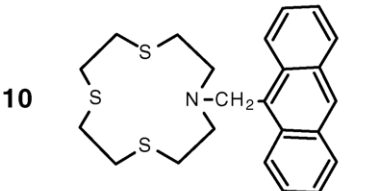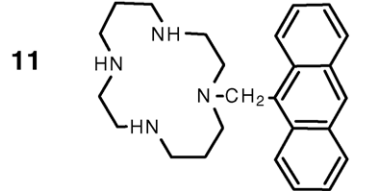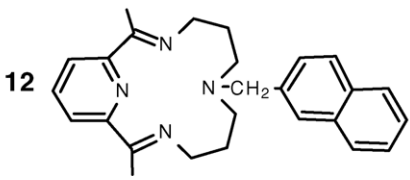
Fig. 8. Two-component molecular fluorescence switches operating through a metal centered redox couple. The metal centre, in a given oxidation state, can quench the emission of the nearby fluorophore through either an eT (electron transfer) or an ET (energy transfer) mechanism.

We mentioned before that whether a two-component system like those listed in Fig. 8 behaves as a switch (ON/OFF, OFF/ON) or not (OFF/OFF, ON/ON) is essentially a matter of chance. Actually, it is not easy to predetermine the quenching mechanism in the OFF state, either electron transfer or energy transfer. However, in the case of the eT mechanism, the OFF/ON behaviour of most of the switches listed in Fig. 8 can be satisfactorily accounted for. In fact, the key term of the switching behaviour is associated with the redox properties of the fluorophore, which, in all the cases considered, was a condensed aromatic molecule: naphthalene or anthracene. It happens that the fluorophore Fl shows a moderate resistance to oxidation (to Fl^+) and a much higher resistance to reduction (to Fl^-). Thus, the eT process from Fl^* to the oxidised metal (which involves the formation of Fl^+) is thermodynamically feasible, whereas the electron transfer from the reduced metal to Fl^* (which involves the formation of Fl^-) is energetically very disfavoured.

3. Metal centred pH fluorescence switches: static and dynamic versions

There exist metal complexes in which the ligand displays acid–base behaviour, releasing/uptaking a hydrogen ion from/to its organic backbone: the protonation/deprotonation process may seriously affect the electronic and stereochemical properties of the metal. We considered that such variations could be exploited for generating a pH fluorescence switch.
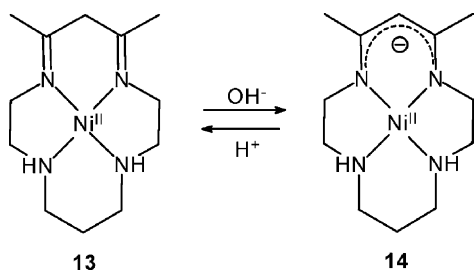
An example is provided by the nickel(II) complex of a 14-membered unsaturated tetra-aza macrocycle (**13**, $[Ni^{II}(HL)]^{2+}$, *diene* form), which, in slightly basic solution, deprotonates, to give the mono-positively charged complex $[Ni^{II}(L)]^+$ (**14**, *dienato* form) [17]. In particular, the hydrogen ion is released from the $-CH_2-$ group in the α-position with respect to the two C=N double bonds of the diene macrocycle **13**, giving rise to a sort of keto-enolic tautomerisation equilibrium. Deprotonation is expected to increase the electron charge density on the metal centre, affecting its redox properties. Moreover, geometrical changes are observed in the ligand framework. In particular, the six-membered chelate ring containing the two C=N double bonds, in **13**, is puckered, due to the tetrahedral hybridisation of the α-carbon atom. In the dienate complex, the same chelate ring, due to π-delocalisation, is planar. Having in mind these properties, we appended to the α-carbon atom, through a bridging $-CH_2-$ group, a naphthalene fragment [18]. The molecular structure
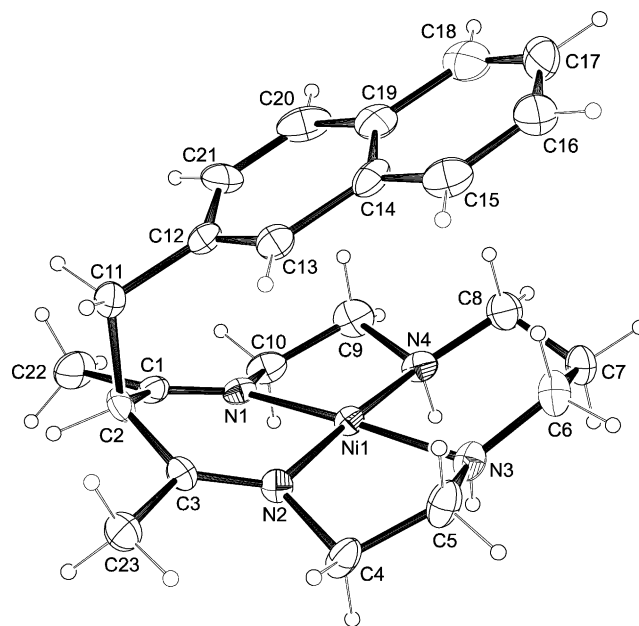

Fig. 9. ORTEP diagram of the $[Ni^{II}L]^{2+}$ complex: L = 5,7-dimethyl-6-naphthalen-2-ylmethyl-1,4,8,11-tetraaza-cyclotetradeca-4,7-diene [18]. The naphthalene fragment is located above the tetra-aza-macrocyclic ring, acting as a roof for the Ni^{II} ion. Such an arrangement may be due the establishment of interactions between the nitrogen atoms of the macrocycle and the aromatic subunit. Reproduced from Ref. [18], with permission of the copyright owners.

of the nickel(II) complex with such a ligand (diene form, $[Ni^{II}(HL)]^{2+}$) is shown in Fig. 9.

The complex displays a rather curious stereochemical arrangement, with the naphthalene subunit bent above the N_4 plane of the macrocycle and forming with it an angle of $26.0°$. As a consequence, the naphthalene fragment looks like a roof protecting the Ni^{II} centre. Ni^{II} is in the low-spin square-planar state, as generally observed with 14-membered tetra-aza-macrocyclic complexes, in the presence of poorly coordinating anions (perchlorate, in the present case). The emissive behaviour is interesting and the diene-dienato equilibrium provides a pH-dependent switch.

In fact, the diene complex **16**, in 4:1 MeCN–water solution, displays typical naphthalene emission. At pH > 8, the emission intensity decreases, to be completely quenched at pH > 10. Going back with pH, from basic to acidic solution, the fluorescence is restored. In particular, fluorescence can be switched ON/OFF consecutively, at will, through the alternating addition of standard acid and base. The acid–base behaviour is characterised by a $pK_A = 8.8$, and its stereochemical aspects are pictorially outlined in Fig. 10. The position of the naphthalene fragment deserves a comment: in the diene complex, **15**, the aromatic subunit resides above the macrocyclic ring, as indicated by X-ray diffraction studies (Fig. 9). No crystallographic data are available for the dienato form, **16**. However, it is supposed that due the change of hybridisation of the α-carbon atom – from sp^3 to sp^2 – the naphthalene fragment is displaced from above the macrocyclic ring to a
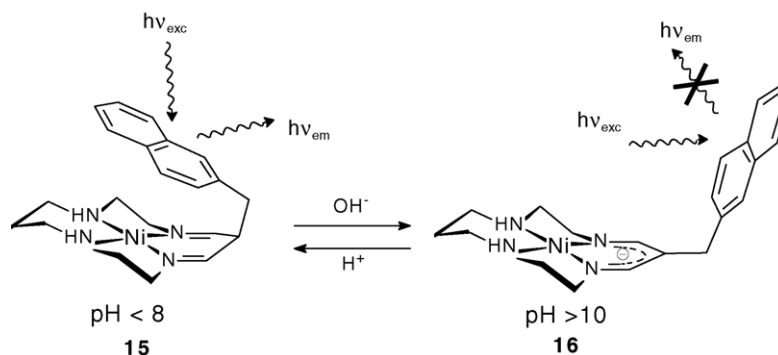
Fig. 10. pH-switching of fluorescence in a Ni^{II} tetra-aza-macrocyclic complex. In the diene form (**15**), fluorescence is ON, in the dienato form (**16**), fluorescence is OFF. Fluorescence quenching in complex **16** is due to the occurrence of an electron transfer process from the Ni^{II} centre to the excited naphthalene fragment. Adapted from Ref. [18].

more distant position. The occurrence of a switching situation – the diene form does not quench naphthalene, the dienato form does – has to be ascribed to the different electron transfer tendencies of the Ni^{II} centre and can be fully accounted for on a thermodynamic basis. In fact, in the dienato complex, **16**, an electron transfer takes place from the Ni^{II} ion to the photoexcited naphthalene fragment. The free energy change associated to the Ni^{II}-to-Naphth* electron transfer process, ΔG°_{eT}, calculated through a thermodynamic cycle of the type shown in Fig. 6, is distinctly negative (-0.2 eV) and accounts for the occurrence of the process. A key term used in the calculation is the electrode potential associated with the Ni^{III}/Ni^{II} couple within **16**: 1.21 V versus SCE, as determined from the reversible cyclic voltammogram in a MeCN solution. On the other hand, no peak for the oxidation of Ni^{II} to Ni^{III} within the diene system **15** is observed up to the solvent anodic discharge, which takes place at 1.8 V. Thus, the potential of the Ni^{III}/Ni^{II} couple in **15** is >1.8 V. It derives that the corresponding ΔG°_{eT} value is >0.4 eV, which explains why the Ni^{II}-to-naphth* electron transfer process does not occur in complex **15** and naphthalene emission remains on. Thus, the fluorescence switching behaviour has to be related to the propensity of the Ni^{II} centre to lose one electron. Such a tendency is ultimately controlled by the overall charge of the complex, whether monopositive in **16** (easier oxidation, fluorophore quenched) or dipositive in **15** (more difficult oxidation, fluorophore unaffected).

In the fluorescence switch described above, the input (either an OH$^-$ or a H$^+$ ion) modifies the electron density on the metal centre, whose interaction with the nearby fluorophore is changed. It is true that the acid–base process also induces a spatial rearrangement (related to the change of hybridisation of the α-carbon atom), but this has no effect on fluorescence switching, which eventually depends on a mere redistribution of electrons. Thus, this switch is defined of the *static* type.

However, pH-controlled switches of fluorescence can also operate in a dynamic way. In particular, the ON/OFF fluorescence switching can be unambiguously associated with a distinct motion taking place within a multicomponent sys-

tem, where a metal centre plays a crucial role. A specific example is provided by metal *scorpionate* complexes.
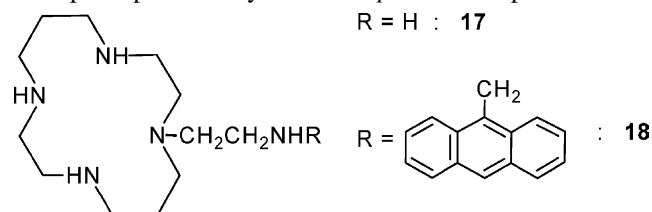
The basic system is a 14-membered tetra-aza macrocycle (cyclam), bearing an ethylamine side-chain, **17** [19]. When a transition metal, e.g. Ni^{II}, is incorporated by the tetramine ring of **17**, the in-plane metal–nitrogen interactions are typically inert, due to the kinetic macrocyclic effect [20], and the metal cannot be extruded from the ring, even in a strongly acidic solution. On the other hand, the pendant arm binds the metal centre from the top, and the M−N bond which forms is labile. Thus, on acidification, the axially bound amine group becomes protonated and the side-chain bearing the ammonium group moves away from the metal centre (Fig. 11).

The process is fast and reversible and the pendant arm can be relocated at will into one of two distinct positions, one on the metal centre, the other remote from it, by means of a fine variation of the pH: $pK_A \pm 1$. In the case of the Ni^{II}–**17** system ($pK_A = 2.8$), the occurrence of the molecular motion can be visually perceived through a neat colour change. At low pH, Ni^{II} exhibits a square-planar coordination, low-spin state, yellow colour; at pH greater than 2.8, the pendant arm
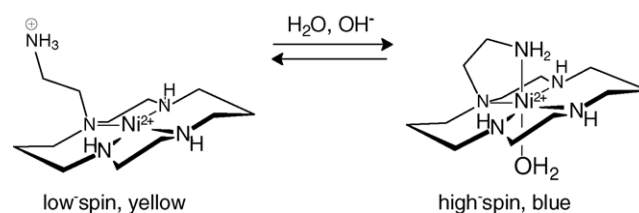

Fig. 11. The pH-controlled molecular movement of the side-chain in a nickel(II) scorpionate complex. The pK_A of the ethylammonium pendant arm is 2.8.
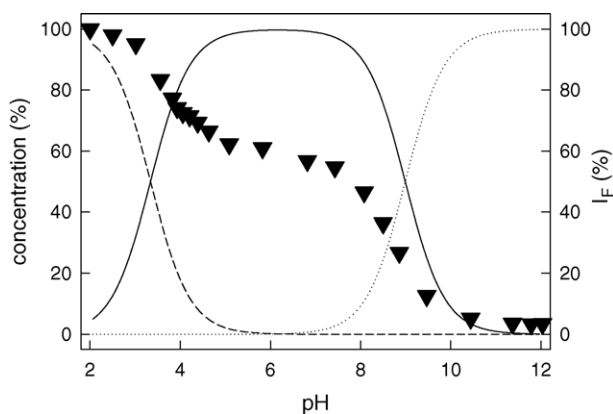
Fig. 12. pH dependence of the relative fluorescence intensity I_F of the anthracene fragment of the Ni^{II} scorpionate complex of ligand **18** (L) (filled triangles, right vertical axis) and distribution curves of the three species present at the equilibrium: [Ni^{II}(LH$^+$)]$^{3+}$, [Ni^{II}(L)(H$_2$O)]$^{2+}$, [Ni^{II}(L)(OH)]$^+$ (dashed, full and dotted lines, respectively; left vertical axis). Adapted from Ref. [21].

occupies one of the axial positions of the coordination octahedron, the other one being taken by a water molecule: the spin state is high, the colour pale blue-violet. The yellow and blue colours can be interconverted at will, through consecutive additions of standard acid and base. Due to the unique feature of an aggressive tail capable of biting an already chelated individual (the metal ion), from the top, ligands of this type were named *scorpionands* [19]. Metal scorpionate complexes provide a clear example of a controllable molecular motion driven by a pH change and based on the metal–ligand interactions.

Noticeably, the molecular movement in a scorpionate complex can be associated with the generation of a luminescent signal. In this perspective, an anthracenyl fragment was appended to the aminoethyl side-chain of **17**, to give **18**, and, very interestingly, the emission of the corresponding Ni^{II} complex was found to be distinctly affected by pH [21].

Fig. 12 displays the variation with the pH of the fluorescence intensity, I_F, of the anthracene subunit of the [Ni^{II}(**18**)]$^{2+}$ complex (filled triangles). The strongest emission is observed at pH ≤ 2. Then, I_F decreases to reach a

plateau, corresponding to 60% of the original emission intensity. A further pH increase induces complete fluorescence quenching (pH ≥ 10). The presence at the equilibrium of three species was assessed through potentiometric titration experiments: (i) a [Ni^{II}(LH$^+$)]$^{3+}$ species, having the side arm protonated (pH ≤ 3); (ii) a [Ni^{II}(L)(H$_2$O)]$^{2+}$ species, in which the amine pendant arm is axially bound, according to a *trans*-octahedral coordinative arrangement, the other axial position being occupied by a water molecule (4 ≤ pH ≤ 8); (iii) a species derived from (ii), through the deprotonation of the axially bound water molecule: [Ni^{II}(L)(OH)]$^+$. The distribution curves of the three species over the 2–12 pH interval are shown in Fig. 12, while the stereochemical features of the three forms in equilibrium are sketched in Fig. 13.

Comparison of the distribution curves and of the fluorescence intensity profile in Fig. 12 indicates that each level of emission intensity corresponds to the existence in solution of a well-defined species. In particular, the strongest emission is due to the [Ni^{II}(LH$^+$)]$^{3+}$ complex (**19**), in which the photoexcited anthracene fragment, An*, is at the longest distance from the Ni^{II} centre (see the sketch in Fig. 13) and the metal–fluorophore interaction is minimised. At pH > 3, the pendant arm occupies one of the axial positions of the coordination octahedron, bringing the An fragment much closer to the metal (see formula **20** in Fig. 13). At this shorter distance, an energy transfer process takes place between Ni^{II} and An*, which reduces the fluorescent emission to 60%. Therefore, the pH-driven motion of the side chain of the scorpionate complex is signalled by a definite decrease of the light emission. On the other hand, the complete quenching of fluorescence which takes places at pH ≥ 9 should not be assigned to any molecular movement, but simply to the release of a proton from the axially bound water molecule of the [Ni^{II}(L)(H$_2$O)]$^{2+}$ complex (**20**). As far as the mechanism is concerned, the decrease of the overall electrical charge of the complex on moving from [Ni^{II}(L)(H$_2$O)]$^{2+}$ (**20**) to [Ni^{II}(L)(OH)]$^+$ (**21**) makes the Ni^{II}-to-Ni^{III} oxidation process feasible, thus making possible the electron transfer process from Ni^{II} to An*. Notice that this process was thermodynamically disfavoured in the [Ni^{II}(L)(H$_2$O)]$^{2+}$ complex (**20**). Thus, the fluorescence quenching observed for the
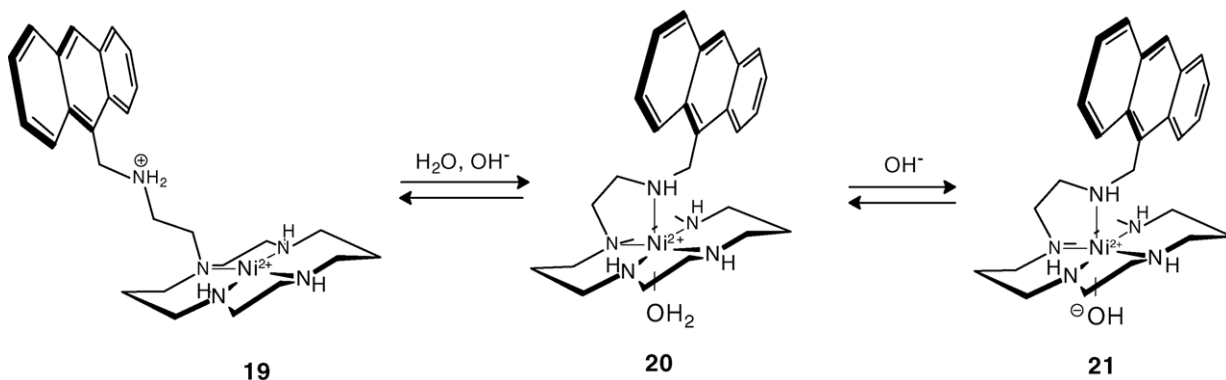

Fig. 13. pH-controlled movement of the fluorescent pendant arm in the Ni^{II} scorpionate complex of ligand **18**. Adapted from Ref. [21].

$[Ni^{II}(L)(OH)]^+$ species (**21**) results from the simultaneous contribution of two different processes: energy transfer and electron transfer (Ni^{II}-to-An^*). The stepwise fluorescence quenching illustrated in the diagram of Fig. 12 is a fast and fully reversible process: on addition of standard acid to the non-luminescent solution at pH = 12, the fluorescence is first restored at 60%, then, at pH ≤ 2, is fully revived. The Ni^{II}–**18** system is an example of a three-position fluorescence switch, driven by a pH change. The motion of the dangling chain is responsible for the switching effect in the acidic region.
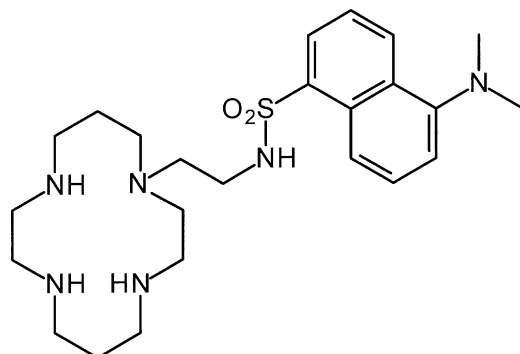
22

In a more recently investigated scorpionand (**22**), the pendant arm contains a sulphonamide group, which belongs to a dansylamide fluorogenic fragment [22]. The sulphonamide group itself is not coordinating: however, at an appropriate pH value, it can deprotonate and bind a given metal centre. This process is made easier if the sulphonamide group is kept permanently close to the metal centre by the $-CH_2CH_2-$ chain of the pendant arm (a manifestation of the chelate effect). Also in the present case, the Ni^{II}–**22** system shows two pK_A values ($pK_{A1} = 4.30 \pm 0.08$ and $pK_{A2} = 7.49 \pm 0.04$ at 25 °C, in an EtOH–water solution, 4:1 (v/v), ionic strength adjusted to 0.1 M with $NaClO_4$), thus indicating the presence of three species in equilibrium, over the 2–12 pH range. If the neutral ligand **22** is indicated with LH, the three species are: $[Ni^{II}(LH)(H_2O)_2]^{2+}$, $[Ni^{II}(L^-)]^+$, and $[Ni^{II}(L^-)(OH)]$.
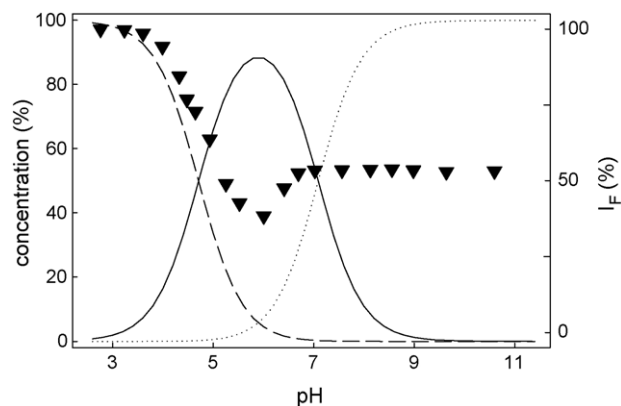

Fig. 14. pH dependence of the relative fluorescence intensity I_F of the dansylamide fragment of the Ni^{II} scorpionate complex of ligand **22** (LH) (filled triangles, right vertical axis) and distribution curves of the three species present at the equilibrium: $[Ni^{II}(LH)(H_2O)_2]^{2+}$, $[Ni^{II}(L^-)]^+$, $[Ni^{II}(L^-)(OH)]^+$ (dashed, full and dotted lines, respectively; left vertical axis). Adapted from Ref. [22].

Fig. 14 displays the percent concentration of the three species in the pH interval investigated.

The two pK_A values refer to equilibria analogous to those observed with the system Ni^{II}–**18** and are illustrated, in their geometrical aspects, in Fig. 15, with some significant differences.

First, the species present in the more acidic region, i.e. at pH < 4.30 (pK_{A1}), in which the pendant arm, in its amide form, is not coordinated, exists as the high-spin, *trans*-octahedral species: $[Ni^{II}(LH)(H_2O)_2]^{2+}$, (**23**). In particular, two water molecules complete six-coordination, occupying the two axial sites of a slightly distorted octahedron. Next, the species existing over the 4.3–7.5 pH interval, in which the deprotonated sulphonamide group is bound to the metal ($[Ni^{II}(L^-)]^+$, scorpionate form), has a five-coordinate trigonal bipyramidal geometrical arrangement (**24**). Such a structural arrangement has been demonstrated by X-ray diffraction
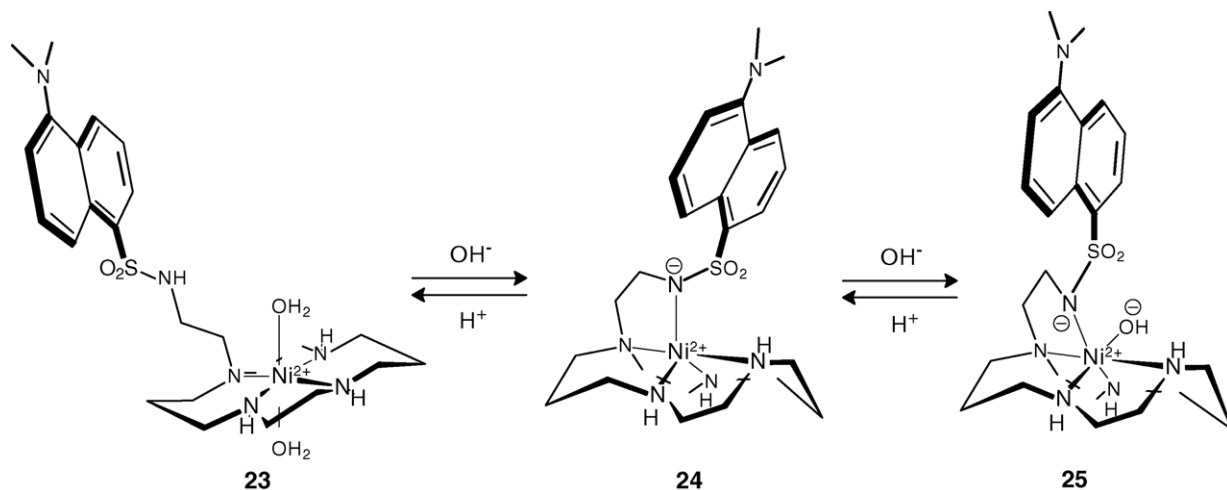

Fig. 15. Geometrical changes associated with the acid–base behaviour of the Ni^{II} complex with ligand **22**. The arrangement of the five-coordinate complex (ii) has been inferred from the molecular structure determined through X-ray diffraction studies (see the ORTEP diagram in Fig. 16). Adapted from Ref. [22].
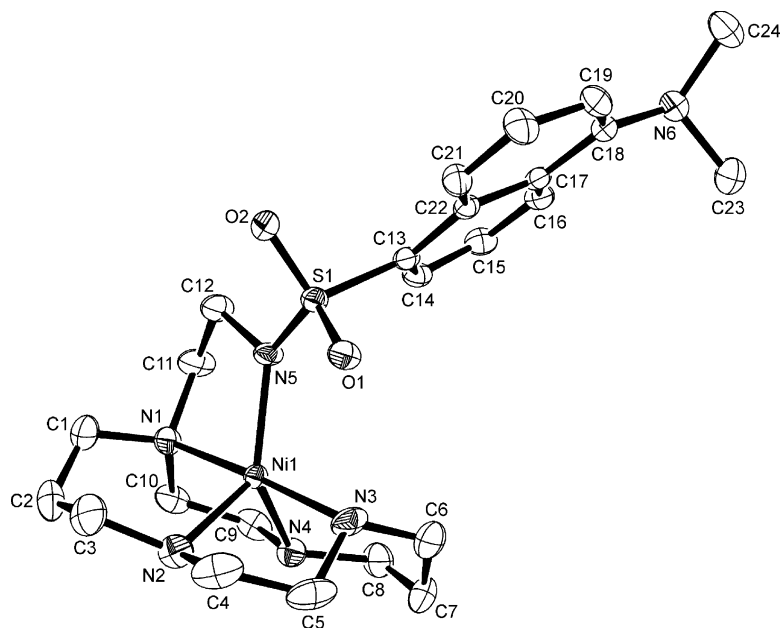
Fig. 16. An ORTEP view of the complex [Ni^{II}(L$^-$)]$^+$, where LH is **22**. The N5 atom belongs to the deprotonated sulphonamide group and occupies one of the corners of the equatorial triangle of a trigonal bipyramid. Reproduced from Ref. [22] with permission of the copyright owners.

studies on a single crystal obtained through slow evaporation of a solution adjusted to pH = 6. An ORTEP view of the [Ni^{II}(L$^-$)]$^+$ complex is shown in Fig. 16.

At pH > 7.5, a neutral species forms: it is suggested that an OH$^-$ ion coordinates to the Ni^{II} centre, inducing a rearrangement to an octahedral species of formula [Ni^{II}(L$^-$)(OH)] (**25**).

The acid–base behaviour of the Ni^{II} complex of **22**, which involves the swinging of the pendant arm (step (**23**) → (**24**) in Fig. 15), has significant effects on the emission behaviour of the dansyl fluorogenic fragment. In fact, the dansyl group itself, when irradiated at 332 nm (absorption of the charge transfer complex), shows a rather broad and unstructured emission band with $\lambda_{max} = 510$ nm. Such an emission band is also present in the fluorescence spectrum of an acidic solution of the Ni^{II} complex of **22** (=L), i.e. a solution of the [Ni^{II}(LH)(H$_2$O)$_2$]$^{2+}$ species. The intensity of such an emission band, I_F, is plotted versus pH in Fig. 14 (filled triangles). It is seen that, in the pH interval 2.5–3.5, I_F maintains its highest value. Then, on raising pH, as the concentration of [Ni^{II}(LH)(H$_2$O)$_2$]$^{2+}$ decreases and that of [Ni^{II}(LH$_{-1}$)]$^+$ increases, I_F diminishes, to reach its minimum value at pH = 6, in correspondence with the highest concentration of [Ni^{II}(LH$_{-1}$)]$^+$. On moving to a higher pH, with the decrease of the concentration of [Ni^{II}(LH$_{-1}$)]$^+$ and the increase of the concentration of [Ni^{II}(LH$_{-1}$)(OH)], I_F grows moderately to reach a plateau at a pH = 7, when the [Ni^{II}(L$^-$)(OH)] species is formed at 100%. This limiting value corresponds to about 50% of the original fluorescence intensity. In summary, full emission of the dansyl fragment is observed in the complex [Ni^{II}(LH)(H$_2$O)$_2$]$^{2+}$ (structure (**23**) in Fig. 15); then, fluorescence is quenched significantly in the complex [Ni^{II}(L$^-$)]$^+$ (**24**); finally, dansyl emission increases moder-

ately in the complex [Ni^{II}(L$^-$)(OH)] (**25**). This behaviour has to be related to different effects exerted by the metal centre on the fluorogenic fragment, in the three different species. In [Ni^{II}(LH)(H$_2$O)$_2$]$^{2+}$ (**23**), the dansyl subunit is far away from the metal and there is no way of establishing through-bond interactions between the Ni^{II} centre and the fluorophore, especially in view of the presence in the chain of an insulating −CH$_2$CH$_2$− spacer: thus, the dansyl group emits its full fluorescence. On the other hand, in [Ni^{II}(L$^-$)]$^+$ (**24**), the Ni^{II} centre can communicate with the aromatic subunit through the coordinative bond and the −NS(O$_2$)− group and can quench the excited fluorophore. It has been demonstrated, through spectrofluorimetric studies at liquid nitrogen temperature, that fluorescence quenching has to be ascribed to an electronic energy transfer process. The electron circulation may be partially reduced in the [Ni^{II}(L$^-$)(OH)] complex (**25**), when the coordination geometry rearranges from trigonal bipyramidal to octahedral and the coordination number changes from 5 to 6. In particular, these changes may induce subtle modifications in the energy of the metal centred orbitals involved in the double electron exchange. It appears that the electronic structure of the five-coordinate complex favours the energy transfer process to a larger extent than observed for the six-coordinate species. The emissive response was found to be quickly reversible, as, on back titration from alkaline to acidic pH, an I_F profile was obtained, which perfectly superimposed on the profile obtained in the direct titration and shown in Fig. 14 (filled triangles).

The two Ni^{II} scorpionand complexes **18** and **22** have in common that the binding of the pendant arm to the metal, when moving from a strongly acidic region to a less acidic pH, is signalled by a distinct decrease of the emission intensity of the covalently attached fluorophore. The two pro-
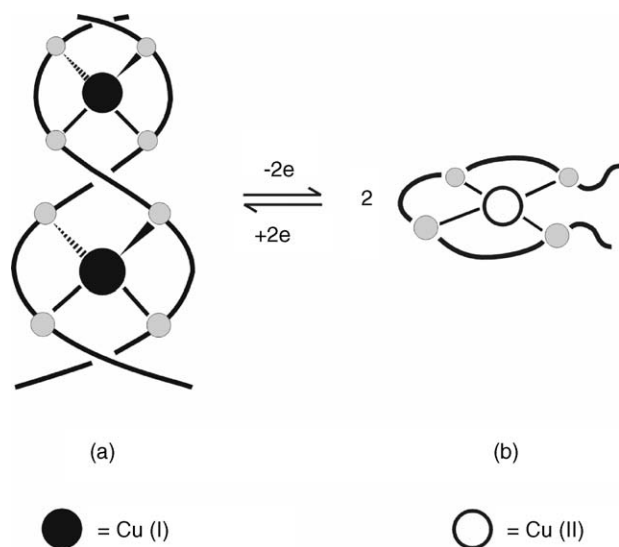
Fig. 17. The disassembling–assembling of a dimetallic helicate, driven by the Cu^I/Cu^{II} redox change. Cu^I likes tetrahedral coordination and favours the assembling of the bis-bidentate ligand to give a double helix (**a**). Such an arrangement is not congruent with the square coordination required by Cu^{II}, whose formation induces disassembling of the dinuclear helicate and formation of two mononuclear complexes (**b**). Reproduced from Ref. [26], with permission of the copyright owners.

cesses take place in different pH intervals due to the different acidic nature of the non-coordinated group of the pendant arm, either more acidic (ammonium in **18**) or less acidic (sulphonamide in **22**).

4. The redox driven assembling–disassembling of helicates

Helicates are polynuclear complexes in which *n* metal ions coordinate two or more strands, each one containing *n* bidentate subunits: the strands have to arrange themselves in a multiple helix [23]. Formation of a polynuclear helicate complex is strictly related to the structural features of the ligands (which must present some elements of rigidity) and to the geometrical requirements of the metal centre acting as a template. In particular, d^{10} cations, which have a preference for tetrahedral coordination, will favour the assembling of two molecules of a bis-bidentate ligand, to give a double-helix arrangement (see structure **a** in Fig. 17).

Changing the oxidation state, when possible, modifies the geometrical preferences of the metal, which may be no longer congruent with the helical assembly. This is the case of the copper centre, whose Cu^I state, d^{10}, prefers tetrahedral coordination and forms a dimeric helicate complex with rigid bis-bidentate ligands (indicated as X∩X, in which X represents a bidentate subunit): [Cu$_2^I$(X∩X)$_2$]$^{2+}$. On the other hand, the contiguous d^9 cation, Cu^{II}, shows a penchant for tetragonal coordination, a geometrical arrangement which does not match the formation of a double helix. Thus, the Cu^I-to-Cu^{II} redox change induces the disassem-

bling of the dicopper(I) helicate into two monomeric subunits, [Cu^{II}(X∩X)]$^{2+}$, sketched as **b** in Fig. 17. The process is fully reversible, so that switching of the metal oxidation state from +2 to +1 and vice versa causes the assembling of the two tetragonal complexes into the double helix, in one direction, and the disassembling of the dimeric system into the monomeric complexes, in the opposite direction. It is possible that, in addition to geometrical reasons, also an electrostatic factor – the increased electrostatic repulsions between the two Cu^{2+} centres – helps the disassembling process.

26   **27**
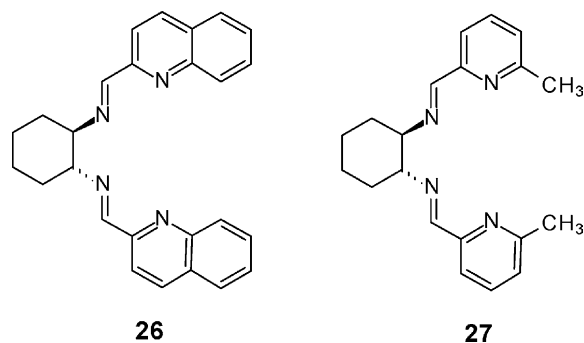
A well-defined case is that of the copper complexes of the quadridentate ligand **26**, which consists of two imine-quinoline halves, linked by a 1,2-cyclohexane spacer [24]. The π-acceptor features of the tetra-aza coordinating set stabilise the Cu^I state, while the relative rigidity of the skeleton disfavours ligand folding to give monomeric complexes: this promotes the formation of a stable dicopper(I) helicate: [Cu$_2^I$(**26**)$_2$]$^{2+}$. However, the stabilisation energy experienced by the Cu^{II} transition metal ion in a square ligating environment helps to overcome the steric obstacles related to the folding of the quadridentate ligand and, on Cu^I-to-Cu^{II} oxidation, the tetragonally coordinated monomeric complex, [Cu^{II}(**26**)]$^{2+}$, forms. Noticeably, species [Cu$_2^I$(**26**)$_2$]$^{2+}$ and [Cu^{II}(**26**)]$^{2+}$ are stable both in solution and in the solid state. In particular, they have been isolated as crystalline salts and their molecular structures have been determined through X-ray diffraction studies [24].

The occurrence of assembling–disassembling in the [Cu$_2^I$(**26**)$_2$]$^{2+}$/[Cu^{II}(**26**)]$^{2+}$ system in an MeCN solution could be followed through cyclic voltammetry investigations. The corresponding CV profile is shown in Fig. 18. The solution contained the cuprous helicate [Cu$_2^I$(**26**)$_2$]$^{2+}$ and the potential of the platinum working electrode was increased from −300 to 900 mV, at a rate of 100 mV s^{-1}. An oxidation peak was observed at ca. 700 mV. Then, on the reverse scan, a reduction peak was observed at ca. 0 mV. The large separation between the two peaks (Δ*p* = 700 mV) can be explained on the basis of the square scheme in Fig. 19.

We start from the bottom right-hand corner of the square, the [Cu$_2^I$(**26**)$_2$]$^{2+}$ helicate complex, at the potential of −300 mV. Going up with the potential, at ca. 700 mV, oxidation to Cu^{II} takes place, with formation of the dimeric [Cu$_2^{II}$(**26**)$_2$]$^{4+}$ form (bottom left). This species is very unstable and disassembles very quickly to give the stable monomeric
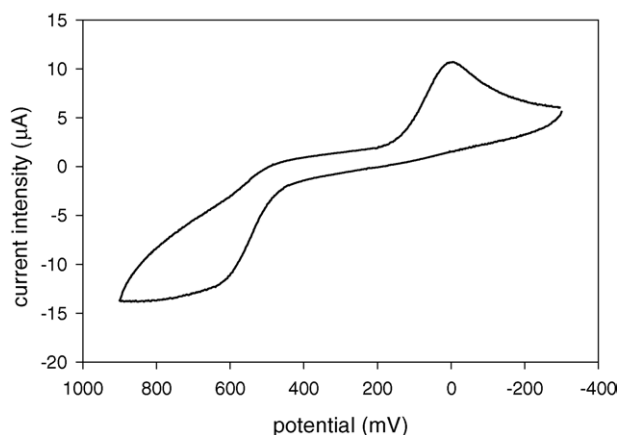
Fig. 18. Cyclic voltammetry profile of an MeCN solution of the helicate complex, $[Cu_2^I(26)_2]^{2+}$, at a platinum working electrode. The potential scan started at -300 mV and was reversed at 900 mV, at a rate of 100 mV s^{-1}. Adapted from Ref. [24].

complex $[Cu^{II}(26)]^{2+}$, upper left corner. At 900 mV the potential is reversed for reduction. However, we do not see any reduction peak at ca. 600 mV, as expected for an electrochemically reversible behaviour (regular peak separation, $\Delta p = 57$ mV): the reason is that we no longer have the dicopper(II) helicate complex to reduce, but the monomeric square species, whose stability is distinctly higher than that of the dicopper(II) helicate and whose reduction takes place at a remarkably more cathodic potential, ca. 0 mV, with a peak separation of 700 mV. The reduction gives the unstable monomeric Cu^I complex, $[Cu^I(26)]^+$, upper-right corner, which immediately assembles to give the helicate: $[Cu_2^I(26)_2]^{2+}$, lower-right corner of the square. Again, oxidation takes place at a much higher potential than expected for the oxidation of the monomeric square Cu^I complex. The overall cycle can be described as an EC + EC sequence of
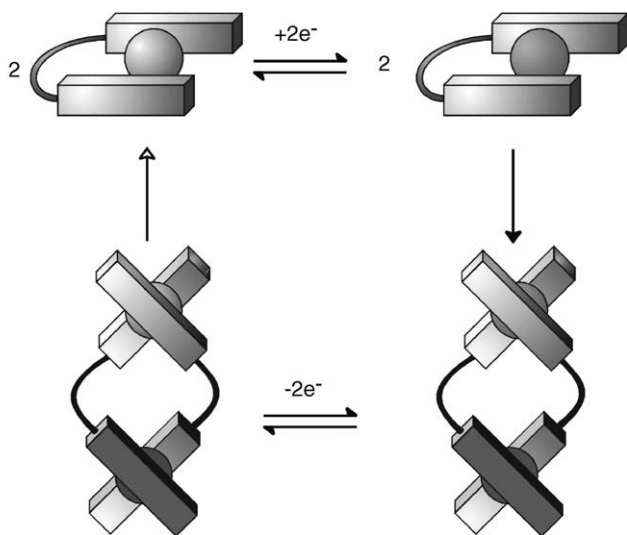
processes (E = electrodic, horizontal; C = chemical, vertical), in which the chemical step C is either assembling or disassembling of the helicate. Each C process is extremely fast and takes place in a time scale much shorter than that of the cyclic voltammetry experiments performed at usual scan rates (50–500 mV s^{-1}). At very high potential scan rates or at very low temperature, it should be possible to 'freeze' the helicate after Cu^I/Cu^{II} oxidation, or the monomeric complex after Cu^{II}/Cu^I reduction, thus obtaining electrochemically reversible profiles ($i_a/i_c = 1$, $\Delta p = 57$ mV, where i_a and i_c are the current intensities of the anodic and cathodic peaks).

In bulk conditions, the occurrence of the redox driven interconversion equilibrium: $[Cu_2^I(26)_2]^{2+} \rightleftharpoons 2[Cu^{II}(26)]^{2+} + 2e^-$, can be followed both visually and spectrophotometrically, as the $[Cu_2^I(26)_2]^{2+}$ complex is red-violet, due to a rather intense absorption band centered at $\lambda_{max} = 530$ nm (MLCT transition, $\varepsilon = 1015$ M^{-1} cm^{-1}), while the $[Cu^{II}(26)]^{2+}$ complex is green (metal centered transition: $\lambda_{max} = 665$ nm, $\varepsilon = 145$ M^{-1} cm^{-1}). The dimer–monomer interconversion can be carried out through exhaustive electrolysis experiments, setting the working electrode at the appropriate potentials. The process is fast and reversible and can be carried out consecutively in either direction. Fig. 20 reports the family of spectra recorded in the course of a controlled potential electrolysis experiment, during the reduction of the monomeric $[Cu^{II}(26)]^{2+}$ complex [25].

Noticeably, both visual and instrumental detection of the assembling–disassembling equilibrium is concentration-dependent. In particular, the interconversion, while clearly perceived at a concentration 10^{-3} M or more, as a red-

Fig. 19. A square scheme illustrating the assembling–disassembling of a dicopper helicate, driven by the Cu^{II}/Cu^I redox couple.
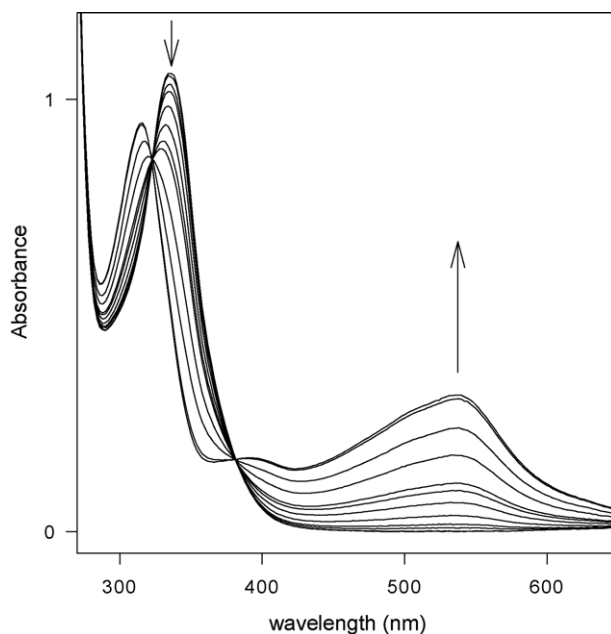

Fig. 20. Electronic spectra of an MeCN solution of $[Cu^{II}(26)]^{2+}$ in the course of a controlled potential electrolysis. On reduction, a band at 550 nm develops (MLCT transition of the $[Cu_2^I(26)_2]^{4+}$ complex), while the band at 340 nm (LMCT of the $[Cu^{II}(26)]^{2+}$ complex) decreases and disappears. Adapted from Ref. [24].

to-green colour change, at 10^{-5} M is observed as a variation from pale pink to colourless. However, the visual (and instrumental) signal can be *amplified* by making use of fluorescence. In this connection, a fluorescent probe was employed in order to monitor the $[Cu_2^I(26)_2]^{2+}/[Cu^{II}(26)]^{2+}$ redox driven interconversion: as an essential prerequisite, such a probe should interfere to a rather different extent with the $[Cu_2^I(26)_2]^{2+}$ and $[Cu^{II}(26)]^{2+}$ forms [26].
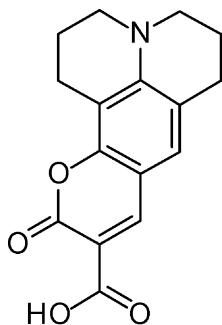
28

The probe employed was the fluorescent fragment **28**, coumarine 343, which, when excited at $\lambda = 420$ nm, emits a yellow light with $\lambda_{max} = 480$ nm. **28** contains a –COOH group, which, when deprotonated, may act as a donor in favour of a coordinatively unsaturated metal centre. In particular, the anion of coumarine 343 gives a five-coordinate 1:1 adduct with the $[Cu^{II}(26)]^{2+}$ complex, in which the emission of the fluorophore is quenched, due to the occurrence of either an electron transfer or an energy transfer process involving the Cu^{II} centre. On the other hand, the coumarine 343 anion does not interact with the helicate complex $[Cu_2^I(26)_2]^{2+}$, in which each metal centre is coordinatively saturated.

On these bases, a solution of $[Cu^{II}(26)]^{2+}$ and of the coumarine anion was electrolyzed at a constant potential. Prior to the electrolysis, the solution was pale yellow (the colour of coumarine) and non-fluorescent. On reduction, the solution began to fluoresce, and an intense band with $\lambda_{max} = 480$ nm developed in the emission spectrum. I_F values measured in the course of the exhaustive reduction are shown, as filled circles, in Fig. 21. On subsequent oxidation, a progressive decrease of I_F was observed. On alternating the potential of the working electrode between the two values, a saw-tooth profile of the fluorescence intensity was obtained, as shown in Fig. 21. Such a behaviour has to be associated with the release (fluorescence ON)—uptake (fluorescence OFF) of the coumarine anion, Fl^-, as long as the copper complexes assemble–disassemble according to the redox equilibrium below:

$$2[Cu^{II}(26)(Fl)]^+ + 2e^- \rightleftharpoons [Cu_2^I(26)_2]^{2+} + 2Fl^-$$
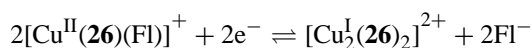
However, progressive signal attenuation was observed in the course of the consecutive reduction and oxidation cycles, which was ascribed to the decomposition at the electrode of the fluorescent indicator. In particular, coumarine 343 is not very stable in an electrochemical sense, undergoing irre-
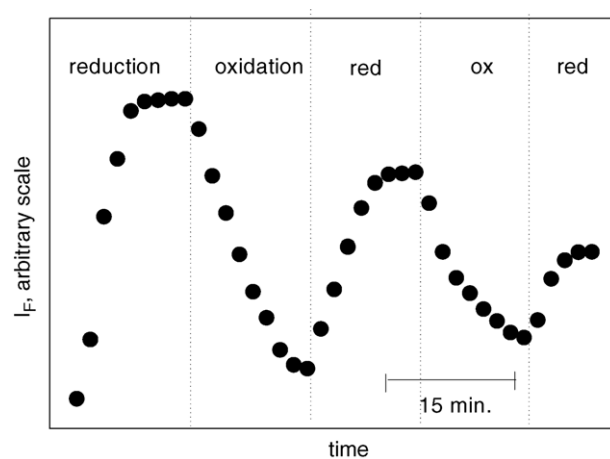
Fig. 21. Fluorescent intensity, I_F, of an MeOH solution 2×10^{-5} M in $[Cu^{II}(26)]^{2+}$ and 2×10^{-6} M in the anion of **28**, in the course of consecutive electrolysis experiments at constant potential. On reduction, the indicator is released to the solution and fluorescence is revived; on oxidation, the indicator is uptaken by the $[Cu^{II}(26)]^{2+}$ complex and fluorescence is quenched. Reproduced from Ref. [26] with permission of the copyright owners.

versible oxidation processes at the platinum electrode. In this connection, the CV profile of coumarine 343 in MeOH 0.1 M $[Bu_4N]ClO_4$ is shown in Fig. 22 (solid line). The first (irreversible) oxidation peak develops at a potential which is almost coincident with the oxidation peak of the $[Cu_2^I(26)_2]^{2+}$ helicate complex (long dash).

In order to avoid the problem of the competitive oxidation of the fluorophore, a dicopper(I) helicate complex whose oxidation–disassembling process takes place at a less posi-
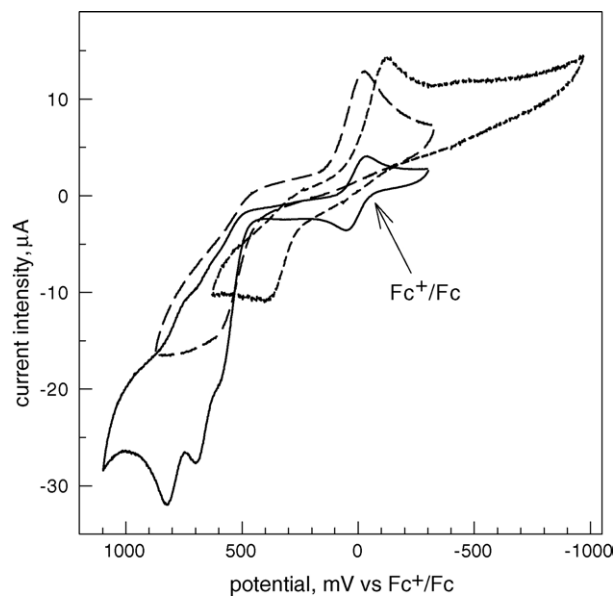
Fig. 22. Cyclic voltammetry profiles for $[Cu_2^I(26)_2]^{2+}/[Cu^{II}(26)]^{2+}$ (long dash) and $[Cu_2^I(27)_2]^{2+}/[Cu^{II}(27)]^{2+}$ (short dash), in MeOH 0.1 M $[Bu_4N]ClO_4$; potential scan rate: 100 mV s^{-1}. The solid line refers to a solution of coumarine 343, to which a small amount of ferrocene had been added, as an internal standard. Reproduced from Ref. [26] with permission of the copyright owners.

Fig. 23. Consecutive reduction and oxidation cycles in a controlled potential electrolysis experiment on an MeOH solution 2×10^{-5} M in $[Cu^{II}(27)]^{2+}$ and 2×10^{-6} M in the anion of **28**. Vertical axis reports the fluorescence intensity, I_F, of **28** in the course of the electrolysis. Reproduced from Ref. [26] with permission of the copyright owners.

tive potential was sought. In particular, in the family of Schiff base ligands derived from *trans*-1,2-cyclohexanediamine, a system exists for which the Cu^I/Cu^{II} oxidation process takes place at a potential distinctly less positive than for $[Cu^I_2(26)_2]^{2+}$: it is the dicopper(I) helicate complex with the bis-bidentate ligand **27**, in which the terminal quinoline fragments have been replaced by 2-methyl-pyridine subunits. The CV profile for the $[Cu^I_2(27)_2]^{2+}/[Cu^{II}(27)]^{2+}$ system is shown in Fig. 22 (short dash). Note that the oxidation peak of $[Cu^I_2(27)_2]^{2+}$ is located at a potential more than 200 mV less positive than that of $[Cu^I_2(26)_2]^{2+}$ (long dash). Moreover, the oxidation peak of $[Cu^I_2(27)_2]^{2+}$ anticipates well the first oxidation peak of coumarine 343 (solid line).
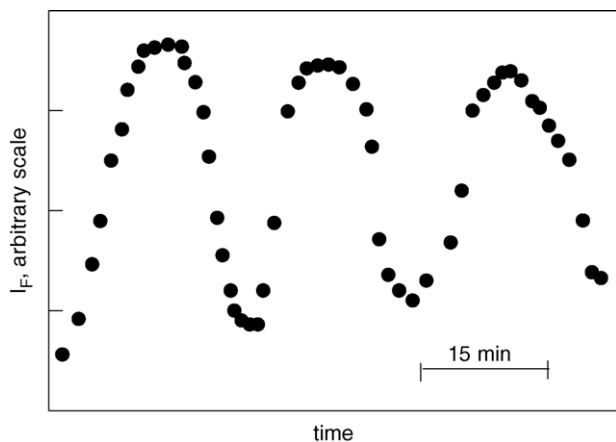
Thus, a controlled potential electrolysis experiment was carried out on an MeOH solution 2×10^{-5} M in $[Cu^{II}(27)]^{2+}$, 2×10^{-6} M in the coumarine anion, and 0.1 M in $[Bu_4N]ClO_4$. In particular, consecutive reduction and oxidation cycles were performed, in which alternating revival-quenching of the coumarine fluorescence corresponded according to a saw-tooth profile (see Fig. 23). Noticeably, the attenuation of the fluorescence signal was much less pronounced than in the case of the $[Cu^I_2(26)_2]^{2+}/[Cu^{II}(26)]^{2+}$ system. This is a beneficial effect of operating the oxidation cycle at a potential low enough to prevent decomposition of the auxiliary fluorescent probe. Moderate signal attenuation is still present, which indicates the occurrence of some oxidative decomposition. Such an effect becomes significant in view of the rather high dilution (μmolar scale) of the fluorophore.

5. pH-driven translocation of metal ions

Scorpionate complexes considered in Section 3 contain a movable part (the pendant arm), whose motion can be

reversibly and repeatedly carried out by taking profit from an external input: a pH change. They convert energy (that of an acid–base reaction) into mechanical work and can be therefore considered *machines* operating at the molecular level [27,28]. Due to the presence of a fluorogenic fragment on the pendant arm, whose emission intensity changes with the motion, these systems can be defined as *light-emitting molecular machines*.

However, there exists another way to induce controlled movements at the molecular level, thus converting the energy of an acid–base reaction into mechanical work. This can be done by moving a particle (e.g. a metal ion) between two distinct sites of a ditopic system, following a predetermined pathway. In order to guarantee fast reversibility, the interaction of the movable particle with either compartment must be labile. Such a feature can be achieved when the particle is a d block metal ion and each compartment is able to establish selective coordinative interactions with it. This can be done by designing a compartment (e.g. A), which displays both coordinating tendencies and Brønsted acid–base properties. As an example, the envisaged compartment should be able to exist both in a protonated form, AH_n, and in a fully deprotonated form, A^{n-}, whereas the second compartment, B, should not show any acid–base feature. Next, the coordinating tendencies of the various compartments should decrease along the series: $A^{n-} > B > AH_n$. Under these circumstances, changing the protonation state of the AH_n/A^{n-} compartment will induce metal translocation [29].

In particular, as illustrated in Fig. 24, when the pH-sensitive compartment is in the AH_n form, M^{n+} will stay in B; but, when the AH_n acid is neutralised to give A^{n-}, M^{n+} will move to the more coordinating deprotonated compartment. Thus, the auxiliary reactions providing the chemical energy for the reversible translocation process are: (i) $AH_n + nOH^- = A^{n-} + nH_2O$ and (ii) $A^{n-} + nH^+ = AH_n$. Noticeably, such acid–base reactions can be carried out through moderate pH changes.
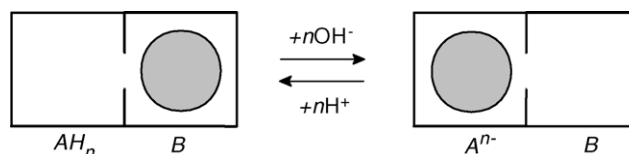
Fig. 24. pH-driven translocation of a metal ion M^{n+} between the two compartments A and B of a ditopic system. Occurrence of metal translocation requires that: (i) compartment A must also exhibit Brønsted acid–base behaviour, according to the equilibrium: $AH_n = A^{n-} + nH^+$; (ii) the affinity towards M^{n+} must decrease along the sequence: $A^{n-} > B > AH_n$. Under these circumstances, the displacement of the acid–base equilibrium, obtained through appropriate pH variations, causes M^{n+} to translocate reversibly between the two compartments. Reproduced from Ref. [30] with permission of the copyright owners.
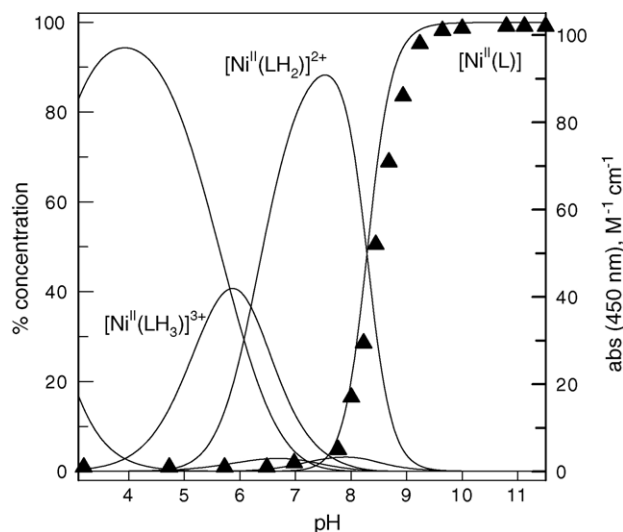
Fig. 25. pH dependence of the percent concentration of the metal complex species for a solution 2×10^{-3} M in **29** (LH$_2$) and 2×10^{-3} M in Ni^{II} (dioxane–water 4:1 (v/v); 0.1 M NaClO$_4$). Filled triangles (right vertical axis) give the molar absorbance of the d–d band at 450 nm, pertinent to the low-spin [Ni^{II}(L)] complex. Adapted from Ref. [30].

29, R =   **30**, R =
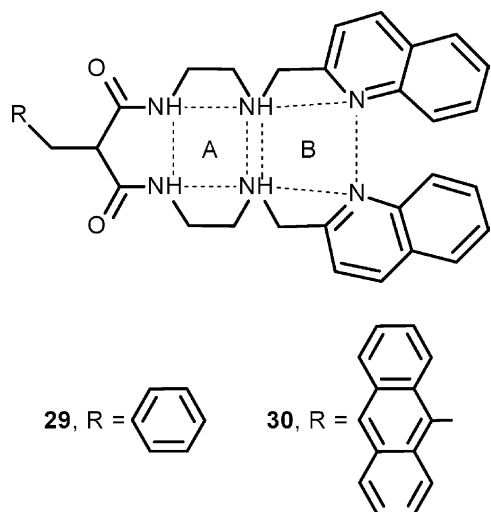
An example of pH-driven metal translocation is provided by system **29**, also indicated as LH$_2$, in which an AH$_2$ compartment is present, which consists of two amine groups and two amide groups [30]. Amide nitrogen atoms displays very poor or nil coordinating tendencies towards transition metals. Thus, compartment AH$_2$ is refused by the metal, which prefers to reside in the more comfortable compartment B, offering two amine groups and two quinoline nitrogen atoms. However, in the presence of divalent metal ions late in the 3d series (e.g. Ni^{II}, Cu^{II}), secondary amide groups, −(CO)NH, may deprotonate, giving rise to the strongly donating group −(CO)N$^-$. In this situation, the M^{n+} ion will move to the more appealing A^{2-} compartment.

Such a behaviour is observed in the case of the Ni^{II} ion. In particular, Fig. 25 illustrates the pH dependence of the concentration of the species present at equilibrium for a solution 2×10^{-3} M both in **29** and in Ni^{II}. Two major

metal complex species are present over the 6–12 pH interval: the complex of the neutral ligand, [Ni^{II}(LH$_2$)]$^{2+}$, and the complex of the doubly deprotonated ligand, [Ni^{II}(L)]. The [Ni^{II}(LH$_2$)]$^{2+}$ complex is present as 90% at pH = 7.5. The absorption spectrum of the solution adjusted at this pH, pale blue in colour, displays two weak d–d bands centred at 606 nm ($\varepsilon = 11$ M^{-1} cm^{-1}) and 820 nm ($\varepsilon = 5$ M^{-1} cm^{-1}), typically observed with a high-spin Ni^{II} ion in an octahedral coordinative environment. This suggests that in the [Ni^{II}(LH$_2$)]$^{2+}$ form the metal centre stays in the B compartment, being equatorially coordinated by the two amine and two quinoline nitrogen atoms. Two water molecules probably occupy the axial positions of a distorted octahedron. On increasing pH, the concentration of [Ni^{II}(LH$_2$)]$^{2+}$ decreases, whereas the [Ni^{II}(L)] complex begins to form, to reach 100% at pH ≥ 9.5. At the same time, the solution takes a bright yellow colour and a band develops at 450 nm ($\varepsilon = 103$ M^{-1} cm^{-1}). Such a band is typically observed with square-planar low-spin Ni^{II} complexes, and is associated with the [Ni^{II}(L)] form, in which the metal centre occupies the A^{2-} compartment and is present in its low-spin form. In particular, it can be observed in Fig. 25 that the profile of the molar absorbance of the yellow low-spin chromophore versus pH superimposes well on the concentration curve of the [Ni^{II}(L)] species. Thus, a pH change from 7.5 (dominating species: [Ni^{II}(LH$_2$)$^{2+}$]) to 9.5 (dominating species: [Ni^{II}(L)]) induces the translocation of the Ni^{II} centre from compartment B to compartment A^{2-} of the ditopic receptor **29**: the intramolecular motion is visually perceived through the colour change of the solution from pale blue to bright yellow, which is due to the occurrence of a drastic rearrangement of the electronic configuration of the metal centre (the Ni^{II} high-spin/low-spin crossover).

The progress of the metal translocation process was followed in real time through a stopped-flow spectrophotometric experiment. In particular, when an aqueous ethanolic solution of [Ni^{II}(LH$_2$)]$^{2+}$ (pH = 7.5) was mixed with an aqueous ethanolic solution buffered at pH = 9.5, a band at 450 nm developed and reached a plateau within less than 1 s. The temporal development of the band pertinent to the [Ni^{II}(L)] complex is illustrated in the diagram in Fig. 26. In particular, the process is first-order, with a lifetime of 0.25 ± 0.01 s.

On the other hand, when the pH of the yellow solution containing [Ni^{II}(L)] (pH ≥ 9.5) is brought back to 7.5, the pale blue colour is quickly restored, indicating that the metal has been translocated again to the B compartment. Stopped-flow spectrophotometric studies indicated that the back translocation is considerably slower than the B to AH$_2$ translocation ($\tau = 2.2 \pm 0.1$ s). Rate difference can be mainly ascribed to the fact that B-to-AH$_2$ translocation involves the dissociation of a high-spin Ni^{II} ion, whereas A^{2-}-to-B translocation involves the dissociation of a low-spin Ni^{II} cation: it is well known that d^8 low-spin metal centres, in a square-planar coordination arrangement, are particularly inert with respect to ligand substitution, due to the high value of the ligand field activation energy.
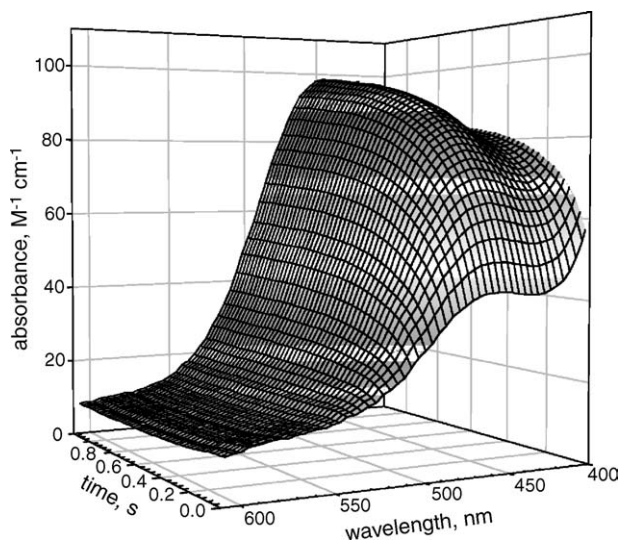
Fig. 26. The family of spectra recorded on a diode array spectrophotometer after the mixing of a solution of $[Ni^{II}(LH_2)]^{2+}$ (pH = 7.5) with a solution buffered at pH = 9.5. Spectra from which the surface originated were taken every 25 ms. Adapted from Ref. [30].

The occurrence of the pH-driven translocation of Ni^{II} within the two-compartment system **29** was followed visually through the appearance–disappearance of the yellow colour (which is due to an electronic d–d transition). We wanted to follow the process through a more effective visual signal, fluorescence. In this perspective, we equipped the framework of the receptor of system **29** with a powerful photoactive fragment: anthracene. In particular, the phenyl ring linked to the AH_2 compartment of **29** was replaced by an anthracenyl substituent, to give **30**.
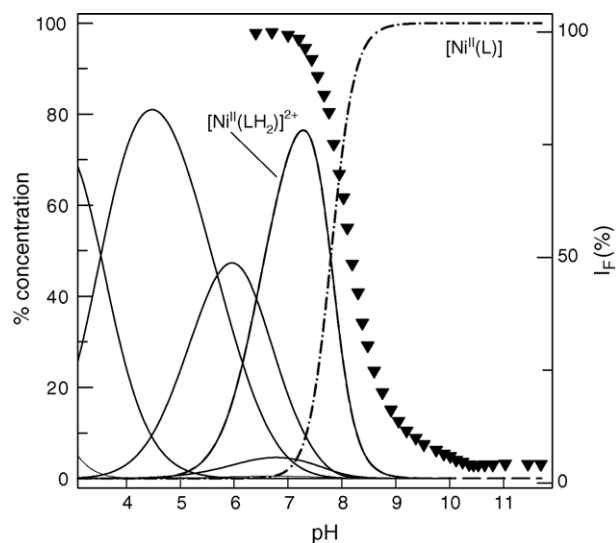

Fig. 27. pH dependance of the percent concentration of the metal complex species for a solution 2×10^{-5} M in **30** (LH_2) and 2×10^{-5} M in Ni^{II} (dioxane–water 4:1 (v/v); 0.1 M $NaClO_4$). Filled triangles (right vertical axis) give the intensity of the fluorescence emission, I_F, for the same solution, when varying pH. Adapted from Ref. [30].

Fig. 27 shows that the same species observed for system **29** are present at the equilibrium over the 2–12 pH range, in a water/dioxane solution (4:1, v/v) containing equimolar amounts of **30** and Ni^{II}. In particular, the $Ni^{II}(LH_2)]^{2+}$ species shows its maximum concentration at pH = 7.5, while the other major species, $[Ni^{II}(L)]$, is present at 100% at pH $\geq$ 9.5. It transpires then that also in the case of system **30**, the Ni^{II} ion can be moved back and forth between the two compartments simply by varying the pH from 7.5 to 9.5 and vice versa. Very interestingly, direct and reverse translocation can be followed by spectrofluorimetry. In particular, it was observed that on increasing the pH of a water/dioxane solution containing equimolar amounts of **30** and Ni^{II}, the intensity of the anthracene (An) emission, I_F, whose values are superimposed on the distribution diagram in Fig. 27, shows its highest value at pH = 7.5, i.e. in correspondence with the $[Ni^{II}(LH_2)]^{2+}$ species. In particular, the emission intensity of the solution of the $[Ni^{II}(LH_2)]^{2+}$ complex is the same as that of a solution of **30** in the absence of metal at the same pH, and comparable to that of plain anthracene under the same conditions. This indicates that the Ni^{II} centre, when in the B compartment, is removed enough from the An fluorophore to prevent interference with its radiative decay. As pH is increased, I_F decreases following a sigmoidal profile, to complete fluorescence quenching at pH $\geq$ 9.5, where 100% of the $[Ni^{II}(L)]$ form is present (see Fig. 27). Thus, the position of the Ni^{II} centre within system **30** is sharply signalled by the emission of the anthracene component: when the metal is in compartment B, fluorescence is ON; when it is in compartment A^{2-}, fluorescence is OFF.

Quenching of the fluorescence of the anthracene fragment is due to the occurrence of a metal-to-fluorophore electron transfer, a process made possible by the easy oxidation to Ni^{III} in the strong ligand field exerted by the deprotonated amide-amine donor set. The occurrence of a Ni^{II}-to-An* electron transfer process is fully accounted for on a thermodynamic basis. In particular, the ΔG°_{eT} value is distinctly negative (-0.35 eV), as calculated from the appropriate combination of the pertinent photophysical ($E^{0-0} = -3.1$ eV) and electrochemical quantities ($eE^0(Ni^{III}/Ni^{II}) = 0.35$ eV; $eE^0(An/An^-) = -2.4$ eV). Thus, the Ni^{II} centre, when in the A^{2-} compartment, quenches the nearby An* fragment through a metal-to-fluorophore eT process. When, following acidification to pH = 7.5, the metal is removed from the A^{2-} compartment and brought back to the B compartment, the electron transfer mechanism vanishes and fluorescence is restored.

The translocation process, both direct and reverse, was followed in its temporal development by monitoring the decay of I_F. The B-to-AH_2 translocation ($\tau = 12 \pm 1$ s) is faster than A^{2-}-to-B back translocation ($\tau = 66 \pm 12$ s), as also observed with system **29**. However, the rates of both direct and reverse processes are remarkably slower for **30** than for **29**. This is ascribed to the presence of the bulky anthracene substituent which slows down the conformational rearrangement experienced by the ligating backbone during translocation. In
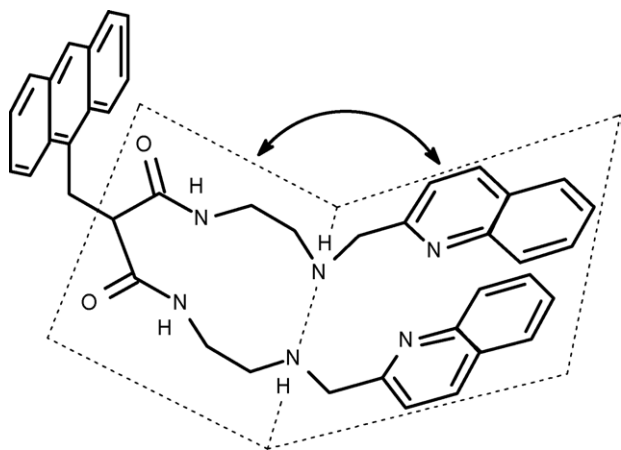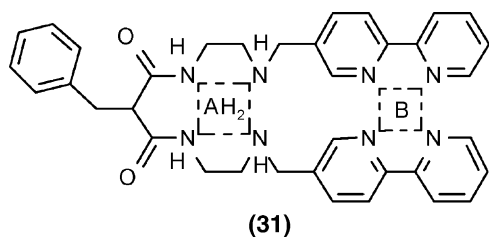
Fig. 28. The 'facing pages' mechanism for the translocation of a metal ion within the two-compartment ligand **30**. Each compartment is placed on one of two facing pages of an ideal book. Metal translocation requires that the two pages are brought to the shortest distance, a situation which corresponds to the transition state.

Fig. 29. Percent concentration of the species present at the equilibrium in a solution containing equimolar amounts of **31** (=LH$_2$) and Cu^{2+} (left vertical axis); profiles **a**, **b**, **c**, and **d** refer to the variously protonated forms of LH$_2$ (from LH$_6^{4+}$ to LH$_3^+$). Profile **e** refers to the metal containing protonated species [Cu^{II}(LH$_3$)]$^{3+}$. Profile **f** refers to the metal containing species [Cu^{II}(LH$_2$)(OH)]$^+$. Filled triangles give the molar absorbance of d–d band ($\lambda_{max} = 502$ nm) of the [Cu^{II}(L)] complex (right vertical axis). Adapted from Ref. [31].

particular, metal translocation may be associated with the occasional folding. It is suggested that the transition state for the translocation process corresponds to a situation in which the two halves of the receptor, placed on the two facing pages of an ideal book, are brought to face each other at the closest possible distance, an event which precedes the metal transfer (see the idealised sketch in Fig. 28). It is probable that the bulky anthracene substituent raises the energy of such a transition state, thus slowing down the rate of both direct and reverse translocation processes.

Also the translocation of a metal ion between the compartments of ditopic ligand can be monitored by means of an auxiliary fluorescent probe, in the same way as the assembling–disassembling of helicates discussed in the previous section. This approach avoids the time-consuming and tedious synthetic procedures required in the covalent linking of the fluorophore to the ditopic ligand.

(31)

System **31** contains a compartment B, consisting of two bpy fragments, which is neatly separated from the diprotic compartment AH$_2$, whose donor set is made of two amine nitrogen atoms and two secondary amide groups. The chosen metal ion is Cu^{II}, which forms a very stable complex with the doubly deprotonated set A^{2-}. On the other hand, compartment B displays fairly good binding tendencies towards Cu^{II}. Moreover, complexes of the [Cu^{II}(bpy)$_2$]$^{2+}$ type tend to be five-coordinate, the remaining coordination site being occupied by a solvent molecule or by a coordinating anion. Thus, it appears that the required sequence of
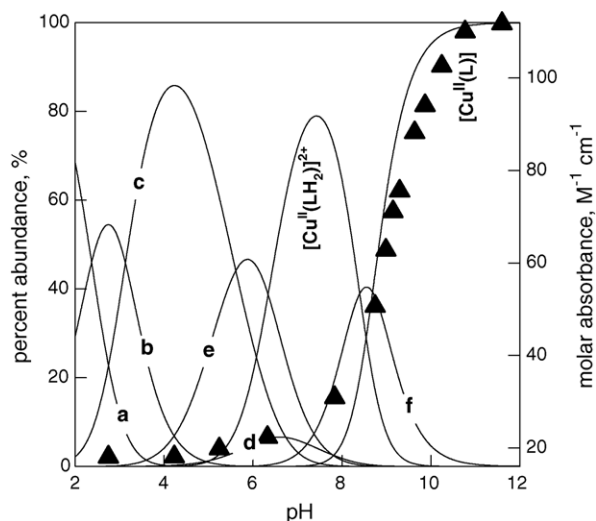
affinity (A^{2-} ≫ B ≫ AH$_2$) is established and that the Cu^{II} ion can be translocated between B and A and vice versa in a defined pH interval.

The complex formation equilibria in a dioxane–water mixture (4:1, v/v) containing equimolar amounts of **31** (LH$_2$) and Cu^{II} were investigated through potentiometric titration experiments. The distribution curves (percent abundance of the species versus pH) of the species present at the equilibrium over the pH interval 2–12 are shown in the diagram in Fig. 29. Two major metal containing species are present beyond neutrality: a species of stoichiometry [Cu^{II}(LH$_2$)]$^{2+}$, which reaches its maximum abundance (80%) at pH = 7.4, and a species of stoichiometry [Cu^{II}(L)], which at pH ≥ 11 reaches 100%. Noticeably, the absorption spectrum of a solution at pH = 7.4, blue in colour, is very similar to that of a solution of the [Cu^{II}(bpy)$_2$]$^{2+}$ model complex, which indicates that, in the complex [Cu^{II}(LH$_2$)]$^{2+}$, the metal stays in compartment B. Due to the tendency of Cu^{II} to reach five-coordination when bound to two molecules of bpy, the complex should be better indicated as [Cu^{II}(LH$_2$)(H$_2$O)]$^{2+}$. On the other hand, bringing pH to 12 by addition of standard base makes the solution become pink-violet (absorption band centred at 500 nm). The colour and the absorption spectrum are those expected for the copper(II) complex of a quadridentate ligand containing two deprotonated amide groups and two amine groups (e.g. dioxo-2,3,2-tet: NH$_2$CH$_2$CH$_2$–NHCO–CH$_2$–CONHCH$_2$CH$_2$NH$_2$). This suggests that in the species dominating at pH ≥ 11, [Cu^{II}(L)], the metal is located in compartment A^{2-}. Very interestingly, the intensity of the band at 500 nm superimposes well on the abundance profile of the [Cu^{II}(L)] species (see Fig. 29).

In conclusion, changing the pH from 7.4 to 12 makes Cu^{II} translocate from B to A^{2-}: the occurrence of the process is signalled by a well detectable colour change: from blue to pink-violet. On addition of standard acid back to pH = 7.4, the solution turns blue again, indicating that the reverse translocation has taken place. The direct and reverse translocation processes can be repeated at will, in principle indefinitely. The detection limit is given by the progressive dilution of the solution, due to the consecutive additions of the standard solution of acid and base.

The rate of the metal translocation, both direct and reverse, was determined by stopped-flow spectrophotometric experiments. In particular, the B-to-A metal displacement was monitored through the development of the absorption band at 500 nm, corresponding to the formation of the pink-violet $[Cu^{II}(L)]$ species. The absorbance versus time profile strictly obeys a first-order kinetics, with a lifetime $\tau = 0.54 \pm 0.05$ s. On the other hand, the first-order A-to-B translocation, investigated through the decay of the band at 500 nm, exhibited a lifetime $\tau = 0.58 \pm 0.05$ s. First-order patterns observed for both direct and reverse processes strongly support the intramolecular nature of the translocation. Please consider that the rates of both direct and reverse translocation are the same, within the experimental error. This is ascribed to the fact that bond dissociation – which probably represents the first step of the translocation process – involves in the present case a cation with the same electronic configuration, d^9, in both directions. On the contrary, in the case of systems **26** and **27**, considered above, remarkable differences were observed in direct and reverse rate, since the translocation involved cations of different electronic configuration and consequently different substitutional properties, depending upon the direction, either d^8 high-spin (from B to A) or d^8 low-spin (from A to B).

In the present case, it was possible to monitor the reversible translocation with the help of an auxiliary light-emitting fragment, which was again coumarin-343, FlH (**28**) [31]. In a 4:1 dioxane–water solution, FlH behaves as a weak acid with a pK_A of 7.30 ± 0.02. The undissociated form FlH is strongly fluorescent with an emission band centred at $\lambda_{max} = 490$ nm; the emission band of the dissociated form, Fl^-, is less intense (fluorescence intensity, I_F, is 75% of that of FlH, and is blue-shifted to a $\lambda_{max} = 471$ nm). Thus, the following experiment was made in order to monitor fluorimetrically the translocation process: first, a solution was made 2×10^{-6} M in coumarin-343, which was found to be fluorescent over the entire pH range, even if a change of I_F and λ_{max} is observed in the 6.5–8.5 pH interval. Then, the same solution was also made 4×10^{-4} M in the copper(II) complex of **31** (i.e. a concentration 220 times higher than that of FlH): as a consequence, a drastic change of the pH dependence of the fluorescence intensity of FlH and Fl^- bands was observed, as shown in Fig. 30.

Fig. 30 shows that, moving from the acidic to the alkaline region, I_F (filled triangles) decreases to be completely quenched at pH = 7–8, then it increases again to reach a

plateau at pH > 11.5, according to a well-shaped profile. This behaviour can be accounted for by considering that in the pH interval corresponding to the well of the I_F profile, the $[Cu^{II}(LH_2)(H_2O)]^{2+}$ species forms and the carboxylate group of Fl^- replaces the water molecule coordinated to the Cu^{II} centre in the B compartment. Binding of Fl^- to the transition metal causes quenching of the fluorescence, through either an electron transfer or an energy transfer process. At pH > 11.5, when more that 99.8% of the metal has translocated to A^{2-}, a square complex is formed which, due to the very strong in-plane interaction, does not exhibit any affinity towards further ligands. As a consequence, Fl^- is released to the solution and displays its full fluorescence. Thus, B-to-A translocation is signalled by the switching ON of fluorescence. On the other hand, A-to-B translocation, induced by bringing pH back to 7–8, is signalled by the switching OFF of the fluorescence. One can go back and forth with pH many times and, due to the greatest efficiency of the fluorescent signal, can perceive each time, both visually and instrumentally, the occurrence of the reversible translocation.

On fitting the spectrofluorimetric data, a binding constant of 5.5 ± 0.1 log units was found for the equilibrium: $[Cu^{II}(LH_2)(H_2O)]^{2+} + Fl^- \rightleftharpoons [Cu^{II}(LH_2)(Fl)]^+ + H_2O$. Thus, it was possible to draw the distribution diagram shown in Fig. 30, which indicates that the $[Cu^{II}(LH_2)(Fl)]^+$ adduct begins to form at pH = 4.5, which causes fluorescence quenching (left arm of the well, full triangles). On the other hand, the decrease of $[Cu^{II}(LH_2)(Fl)]^+$ concentration, associ-
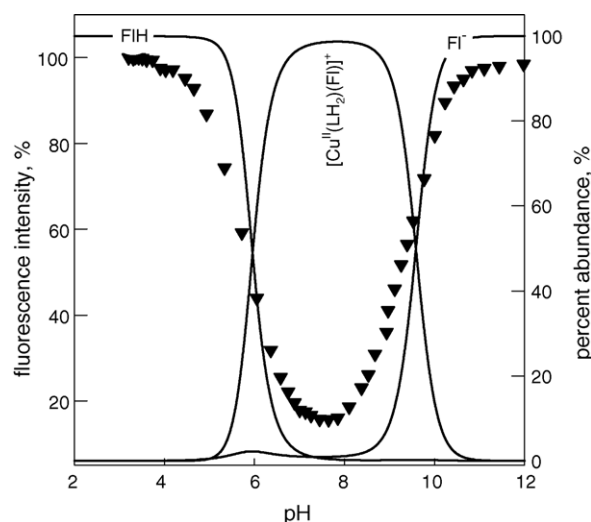
Fig. 30. Full triangles (left vertical axis) indicate the fluorescence intensity, I_F, of a solution 2×10^{-6} M in coumarin-343 (**28**) and 4×10^{-4} M in the $[Cu^{II}(LH_2)]^{2+}/[Cu^{II}(L)]$ complex ($LH_2 = $ **31**). Values of the descending arm of the well-shaped profile refer to the emission band at 490 nm (emitting fragment: undissociated form, FlH); values of the ascending arm refer to the emission band at 471 nm (emitting fragment: dissociated form, Fl^-). I_F values are normalised. Solid lines (right vertical axis) give the pH dependence of the concentration of FlH, $[Cu^{II}(LH_2)(Fl)]^+$, and Fl^-, in the same solution. Moving up from pH = 7, fluorescence OFF (bottom of the well) signals that Cu^{II} stays in compartment B, fluorescence ON signals that Cu^{II} is in compartment A. Adapted from Ref. [31].

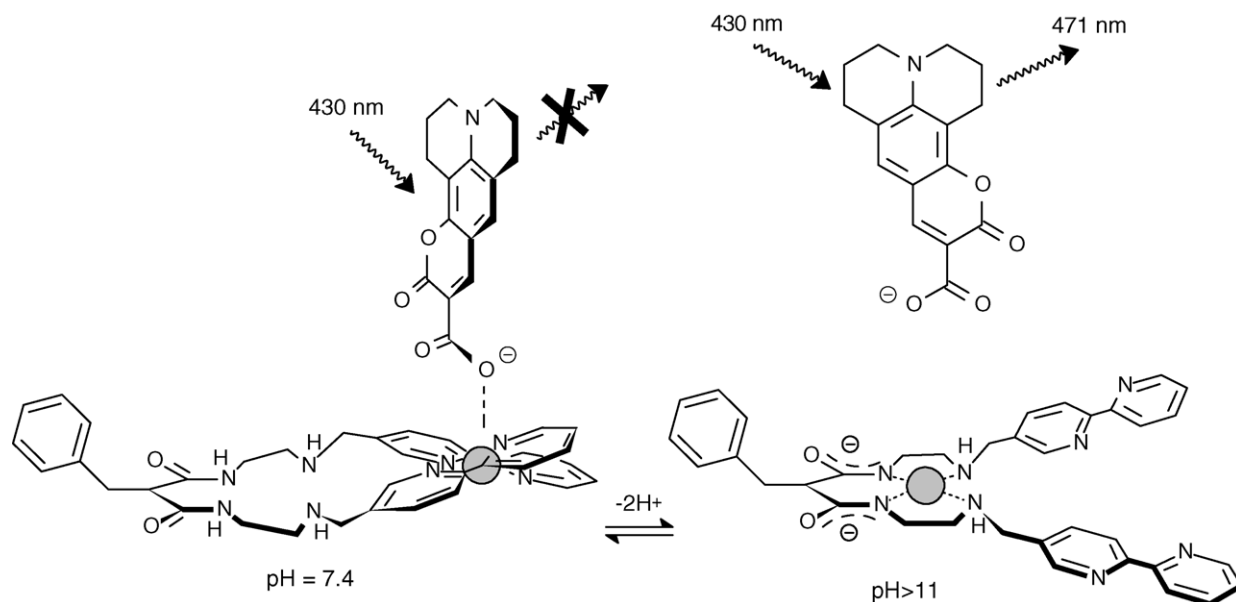Fig. 31. Metal translocation monitored by an auxiliary fluorescent probe. When the Cu[II] centre stays in the (bpy)$_2$ compartment, it is coordinated by the carboxylate group of coumarine-343, whose emission is quenched (fluorescence OFF). On moving to the diamine-deprotonated diamide compartment, the metal is definitively happy with square coordination, and the anion of coumarine-343 is released to the solution, displaying its full emission (fluorescence ON). The state of the fluorescence, whether OFF or ON, signals the position of the Cu[II] centre. Adapted from Ref. [31].

ated with translocation to A, corresponds to the release of the Fl$^-$ light-emitting species and to the revival of fluorescence (right arm of the well, full triangles). Finally, Fig. 31 provides a pictorial sketch of the supposed geometrical aspects of metal translocation and of complexation–decomplexation of Fl$^-$.

6. Light-emitting devices based on the [Zn^{II}(tren)]$^{2+}$ fragment

Tris-(aminoethyl)amine (tren) is a ligand which imposes on the bound metal centre a trigonal bipyramidal geometry. In particular, the tripodal ligand occupies four positions of the coordination polyhedron, leaving an axial site available for coordination by either a solvent molecule or an anion X$^-$ (**32**).

32
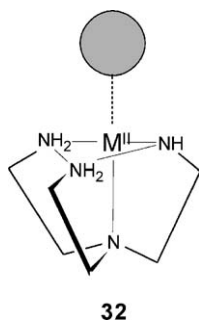
The [Zn^{II}(tren)]$^{2+}$ fragment can be used to build photophysical devices responsive to a chemical input. The zinc(II) centre plays an essential role, as it is coordinatively unsat-
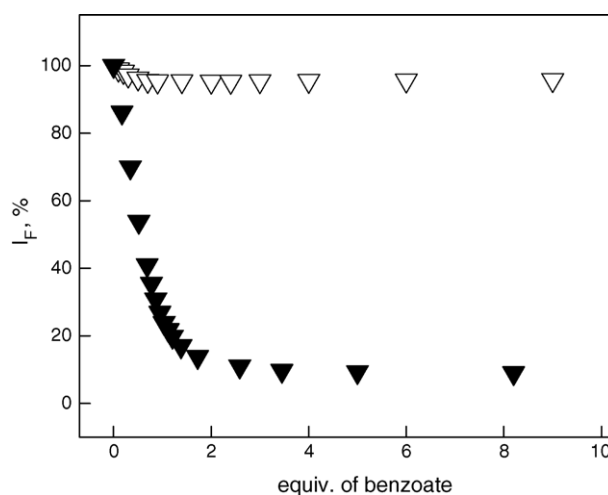
Fig. 32. Spectrofluorimetric titrations of the [Zn^{II}(**33**)]$^{2+}$ receptor in a methanolic solution (10^{-4} M) with standard methanolic solutions of: benzoate (open triangles) and *N,N*-dimethyl-aminobenzoate (filled triangles). Fluorescence intensity, I_F, was taken at 415 nm.

urated and offers room for the coordination of an anion (the chemical input). On the other hand, Zn^{II} is photophysically inoffensive, as (i) it is redox inactive and cannot be involved in any photoinduced electron transfer and (ii) has a closed shell electronic configuration (3d^{10}) and cannot participate in any electronic energy transfer mechanism. Thus, it can exert a useful architectural function, without interfering with photophysically active substituents present on the ligand framework. Substituted tetramines **33**–**35** were studied which allowed us to play some games with fluorescence.

33   **34**   **35**
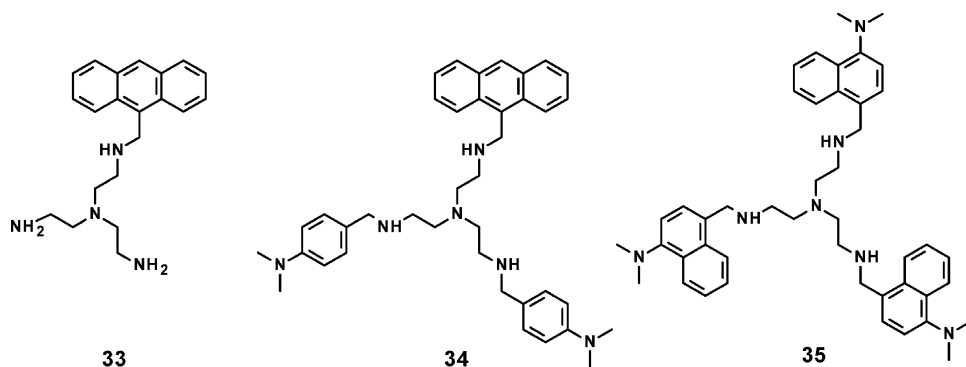
First, the $[Zn^{II}(\mathbf{33})]^{2+}$ was considered, which, in a methanolic solution, displays the typical blue fluorescence of the anthracene fragment [32]. Spectrophotometric titration experiments showed that the $[Zn^{II}(\mathbf{33})]^{2+}$ system forms a stable 1:1 adduct with the benzoate ion in an ethanolic solution, as shown by significant modifications in the UV absorption spectrum. On the other hand, when the titration was carried out within the spectrofluorimetric cuvette, no change was observed in the emission band of the anthracene fragment, even after the addition of several equivalents of benzoate (see open triangles in the titration profile reported in Fig. 32).

Thus, the anthracene subunit witnesses in silence the anion binding to the Zn^{II} centre. However, on titration with 4-*N,N*-dimethylaminobenzoate, X^-, the intensity of anthracene emission band, I_F, progressively decreased until full quenching. The I_F versus X^- equivalents plot (filled triangles in Fig. 32) indicated the formation of a 1:1 adduct, $[Zn^{II}(\mathbf{33})X]^+$ and non-linear least squares treatment of titration data gave a $\log K$ value of 5.45 ± 0.03 for the anion complexation equilibrium: $[Zn^{II}(\mathbf{33})]^{2+} + X^- \rightleftharpoons [Zn^{II}(\mathbf{33})X]^+$. This time, the anthracene fragment receives the information on the occurrence of the metal–benzoate interaction and duly fulfils its signalling function. The question is how the information is transmitted. It is suggested that fluorescence quenching is due to an intramolecular electron transfer process within the $[Zn^{II}(\mathbf{33})X]^+$ adduct, in particular from the metal bound 4-*N,N*-dimethylaminobenzoate subunit to the photoexcited anthracene fragment, An*. In fact, *N,N*-dimethylaniline (DMA) is a well-known electron donor and the free energy change ΔG°_{eT} associated with the DMA-to-*An electron transfer process, calculated through a thermodynamic cycle analogous to that reported in Fig. 6, is distinctly negative (-0.4 eV) and accounts for its feasibility. The mechanism of such a process is pictorially illustrated in Fig. 33.

Quenching of the excited anthracene fragment of the $[Zn^{II}(\mathbf{33})]^{2+}$ receptor is not restricted to 4-*N,N*-dimethylaminobenzoate, but can be observed for any benzoate anion bearing either a *donor* or an *acceptor* group, provided that the thermodynamic requirements for the transfer of an electron *to* or *from* the photoexcited fluorophore are fulfilled. In particular, titration of $[Zn^{II}(\mathbf{33})]^{2+}$ with 4-nitrobenzoate ion in a methanolic solution induces the decrease and quenching of the fluorescence, according to a profile analogous to that displayed in Fig. 32. Nitroben-

zene is a classical acceptor. Thus, fluorescence quenching has to be ascribed to an intramolecular electron transfer process from An* to the metal bound 4-nitrobenzoate anion. The negative value of the ΔG°_{eT} quantity (-1.0 eV) accounts for its thermodynamic feasibility. Quite interestingly, decrease and almost complete quenching of the fluorescence is also observed when $[Zn^{II}(\mathbf{33})]^{2+}$ is titrated with 9-anthracenoate anion. Notice that 9-anthracenoate itself is fluorescent. It is suggested that fluorescence quenching originates from an ET process between the two anthracene subunits of the supramolecular adduct: $^*An + An = An^- + An^+$. Both the anthracenoate-to-anthracene and anthracene-to-anthracenoate electron transfer processes exhibit a slightly negative ΔG°_{eT} value (-0.2 eV). The $[Zn^{II}(\mathbf{33})]^{2+}$ system is able to signal the binding of other carboxylate anions than benzoates, provided that they have definite donor or acceptor tendencies in a photophysical sense. For instance, fluorescence quenching is observed also on titration of
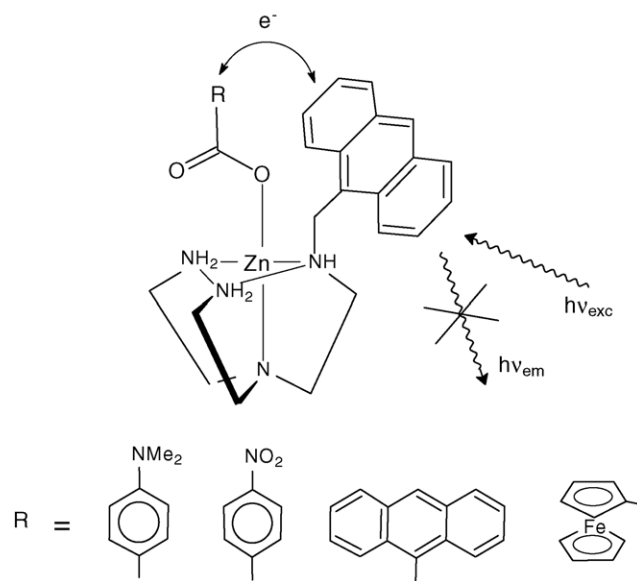

Fig. 33. The intramolecular electron transfer process responsible for fluorescence quenching of the anthracene subunit and for signalling the binding of the carboxylate anion to the Zn^{II} centre. R = 4-*N,N*-dimethylaminophenyl (Donor, D), 4-nitrophenyl (Acceptor, A), 9-anthracenyl (D or A), 1-ferrocenyl (D). Adapted from Ref. [32].

$[Zn^{II}(33)]^{2+}$ with 1-ferrocenecarboxylate. Ferrocene and its derivatives are quite strong donors. In particular, the ferrocene to *An electron transfer is thermodynamically favoured: $\Delta G^{\circ}_{eT} = -0.4$ eV.

Thus, the $[Zn^{II}(33)]^{2+}$ system represents a fluorescent device whose emission can be switched off through a chemical input, an R–COO$^-$ anion whose substituent R presents donor or acceptor tendencies. The process is controlled by the coordinative interaction between Zn^{II} and the carboxylate group which brings the R fragment close enough to the photoexcited anthracene fragment to afford the occurrence of an electron transfer process.

A different game can be played with the zinc(II) complex of the tren derivative **34** [33]. In this case, the tripodal ligand contains both the fluorogenic fragment (anthracene) and the electron donor subunits (*N,N*-dimethyl-aniline), covalently linked, through a —CH$_2$— group, to the peripheral nitrogen atoms of the tren framework. Noticeably, on formation of the $[Zn^{II}(34)]^{2+}$ complex, the anthracene fluorescence is completely quenched. This is due to the occurrence of an intramolecular electron transfer process from one of the DMA substituents to the photoexcited anthracene fragment. Coordination of the tripodal tetramine to Zn^{II} plays an essential role, as it brings the two subunits at a convenient distance. The idea is now that of interrupting the electron transfer, and reviving anthracene emission, through the coordination to Zn^{II} of a carboxylate group bearing a bulky and insulating substituent. The scheme is illustrated in Fig. 34.

In this perspective, an ethanolic solution of the $[Zn^{II}(34)]^{2+}$ complex, non-fluorescent, was titrated with a series of R–COO$^-$ anions, in which R is a substituent of varying bulkiness. The profiles of the spectrofluorimetric titrations are shown in Fig. 35.

First, the solution of the $[Zn^{II}(34)]^{2+}$ complex was titrated with a standard solution of acetate, but this did not induce any increase of fluorescence, indicating that the DMA-to-An* electron transfer process still continued. No fluorescence increase was observed also on titration with the bulkier cyclohexylcarboxylate anion. A moderate increase
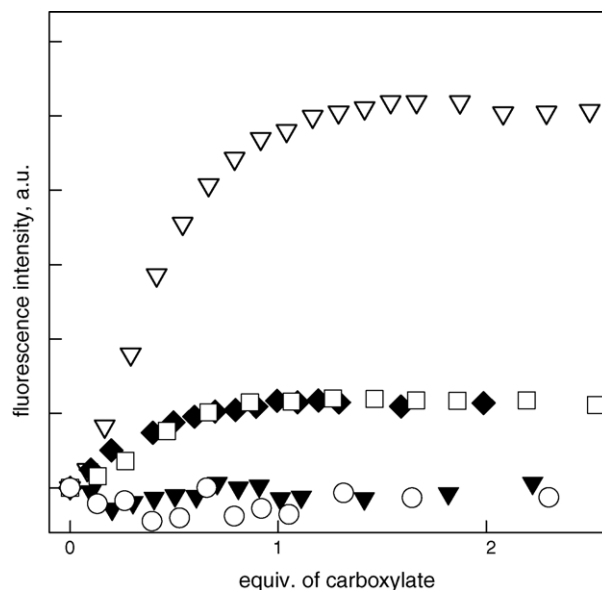
Fig. 35. Titration of a methanolic solution of the $[Zn^{II}(34)]^{2+}$ complex, whose fluorescence is quenched, due to the occurrence of an intramolecular electron transfer process. Titration with acetate (filled triangles) and cyclohexylcarboxylate (open circles) does not induce any fluorescence revival. A moderate fluorescence restoration is observed on titration with 1 adamantanecarboxylate (open squares) and benzoate (filled diamonds). Full fluorescence revival is obtained on titration with 1,1,1-triphenylacetate (open triangles). Adapted from Ref. [33].

of fluorescence (due to the diminished occurrence of the electron transfer process) was observed following titrations with benzoate and 1-adamantanecarboxylate. Full restoration of anthracene fluorescence was obtained upon titration with 1,1,1-triphenylacetate (TPA). The titration profile (open triangles in Fig. 35) clearly indicates the formation of a 1:1 adduct between $[Zn^{II}(34)]^{2+}$ and TPA. A hypothetical structural sketch of the $[Zn^{II}(34)(TPA)]^+$ adduct, which was inspired from semiempirical molecular modeling, is shown in Fig. 36.

A rather simple explanation of this effect is that the TPA anion behaves as an insulating block, which plugs up the electron transfer from one of the DMA substituents to the An* fragment. In the absence of direct structural evidence (e.g. X-ray diffraction data), one could argue that electron transfer interruption is a consequence of a conformational rearrangement of the DMA and An substituents, following TPA coordination to Zn^{II}. However, such an effect is not observed with the bulky 1-adamantanecarboxylate anion, which induces only a moderate increase of the fluorescent emission. On the other hand, it appears that the insulating effect is not only a consequence of the steric hindrance, but it should be in some way related to the presence of aromatic substituents on the incoming carboxylate anion. In fact, the simple benzoate anion exerts a moderate, still detectable effect on inhibiting electron transfer and restoring fluorescence. Such an effect is not produced by coordination of the 'greasy' cyclohexylcarboxylate, which presents a size similar to benzoate.
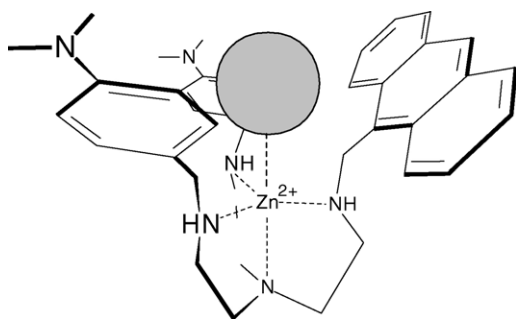

Fig. 34. Occurrence of an electron transfer process from one of the *N,N*-dimethylaniline substituents to the nearby excited anthracene fragment, in the $[Zn^{II}(34)]^{2+}$ complex, causes fluorescence quenching. Coordination of Zn^{II} by a bulky and insulating anion is expected to interrupt the electron transfer and revive fluorescence.
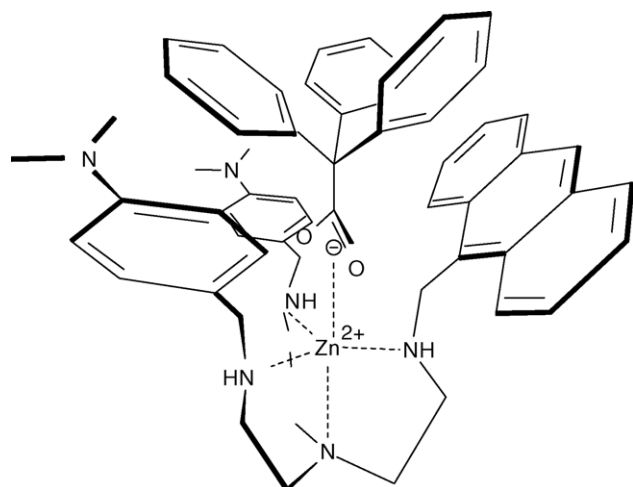
Fig. 36. The proposed structure of the $[Zn^{II}(34)(TPA)]^+$ adduct (TPA = 1,1,1-triphenylacetate). The bulky carboxylate anion stops the electron transfer from one of the *N,N*-dimethylaniline substituents to the photoexcited anthracene fragment, which can now release its full fluorescence.

In conclusion, system $[Zn^{II}(34)]^{2+}$ possesses a built-in electron transfer mechanism, which prevents emission by the fluorophore: coordination by an appropriate anion interrupts the process and restores fluorescence (OFF/ON device). In this sense, the system $[Zn^{II}(34)]^{2+}$ shows an opposite activity with respect to system $[Zn^{II}(33)]^{2+}$, which was per se fluorescent and whose emission was stopped, following coordination of a carboxylate anion which initiated the electron transfer mechanism.

A third game we were interested to play with the Zn^{II} complex of a substituted tren molecule referred to the electronic energy transfer (EET) [34]. In this process, photonic energy is transferred from an excited fragment Fl_1 (adsorbing light at λ_1 wavelength) to a proximate fragment Fl_2, which emits light at a distinctly higher wavelength λ_2. A typical mechanism involves the occurrence of a double electron transfer process between Fl_1 and Fl_2, in a cyclic fashion, and requires that the two fragments experience occasional Van der Waals contacts, so that their orbitals can overlap. Intramolecular EET can be achieved in supramolecular systems, in which Fl_1 and Fl_2 belong to distinct moieties held together by non-covalent interactions (e.g. metal–ligand interactions). In particular, we designed a situation in which Fl_1 is a fragment covalently linked to a peripheral nitrogen atom of the tren framework and Fl_2 is the R substituent of an R–COO$^-$ anion which coordinates to the Zn^{II} centre. In this sense, the tren platform was equipped with three luminescent fragments absorbing UV light (*N,N*-dimethylamine-1-naphthalene: Fl_1; absorption band centred at $\lambda_{max} = 330$ nm, emission band centred at $\lambda_{max} = 424$ nm, due to an internal charge transfer excited state), to give **35**. On the other hand, the dye coumarine-343 (**28**), which shows a strong emission at $\lambda_{max} = 475$ nm and brings a carboxylic function, was chosen as Fl_2. Substantial overlap of the emission band of the *N,N*-dimethylamine-1-naphthalene fragment (Fl_1) and of the absorption band of
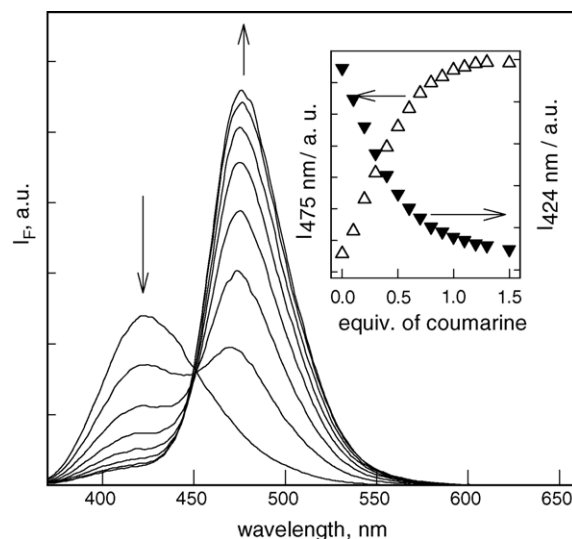

Fig. 37. Emission spectra of an ethanolic solution of $[Zn^{II}(35)]^{2+}$, when titrated with a standard solution of coumarine-343 (**28**). The band at 424 nm (*N,N*-dimethylamine-1-naphthalene fragment) decreases, while the band at 475 (coumarine-343) increases, indicating the occurrence of an electronic energy transfer process. Adapted from Ref. [34].

coumarine-343 (Fl_2) supports the occurrence of an EET process.

An ethanolic solution of $[Zn^{II}(35)]^{2+}$, when irradiated at 330 nm, emits light at 424 nm, due to the radiative decay of the *N,N*-dimethylamine-1-naphthalene fragment Fl_1. Titration with a standard solution of coumarine-343, Fl_2 induced a progressive decrease of the emission band of Fl_1 and the development of an emission band at 475 nm, indicating Fl_2 sensitisation and the occurrence of an EET process involving Fl_1 and Fl_2 (see Fig. 37).

The profiles of the fluorescence intensity, I_F, of both the band at 424 nm (decreasing) and of the band at 475 nm (increasing, see inset in Fig. 34) versus equivalents of Fl_2 correspond to the formation of a 1:1 adduct between $[Zn^{II}(35)]^{2+}$ and coumarine-343. The log K value for the adduct formation equilibrium is 5.98 ± 0.04 (when calculated at $\lambda = 335$ nm) and 6.01 ± 0.03 (at $\lambda = 475$ nm). This behaviour can be explained by considering that coordination to the metal brings the photoexcited Fl_1 substituent close enough to Fl_2 to ensure the occurrence of an efficient EET process, thus leading to a substantial sensitisation of Fl_2 emission. The mechanism of the process is pictorially illustrated in Fig. 38.

7. A molecular fluorescent thermometer

In the previous sections, it has been shown how, in a given molecular system, a chemical input (H$^+$ or OH$^-$ ions, an oxidising or reducing agent) could be translated into a luminescent signal. The molecular system typically consisted of a subunit sensitive to the chemical input and a fluorogenic fragment. We want to describe now an analogous system capable of translating a physical input – temperature – into a light
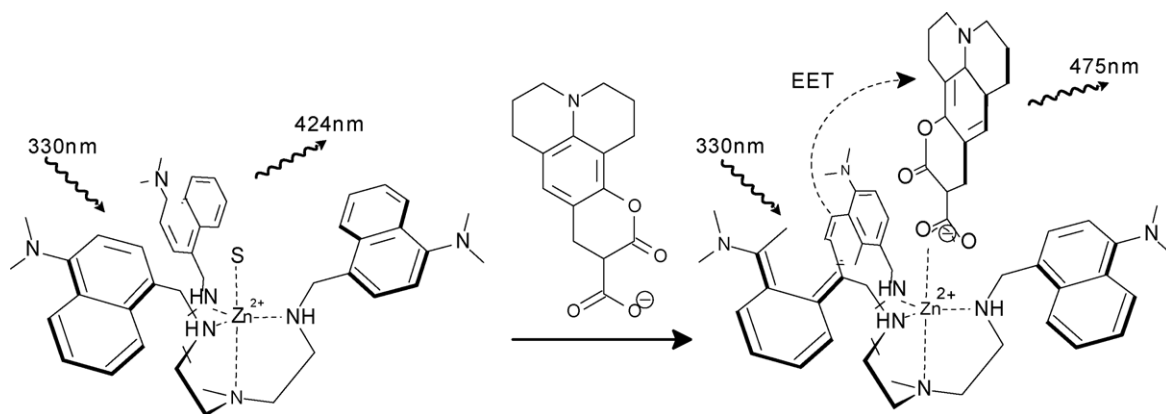
Fig. 38. Electronic energy transfer (EET) from the N,N-dimethylamine-1-naphthalene fragment (Fl₁) to the dye coumarine-343 (Fl₂). Coordination of the dye to Zn^II brings Fl₁ close enough to Fl₂ to permit the EET process to occur. Adapted from Ref. [34].
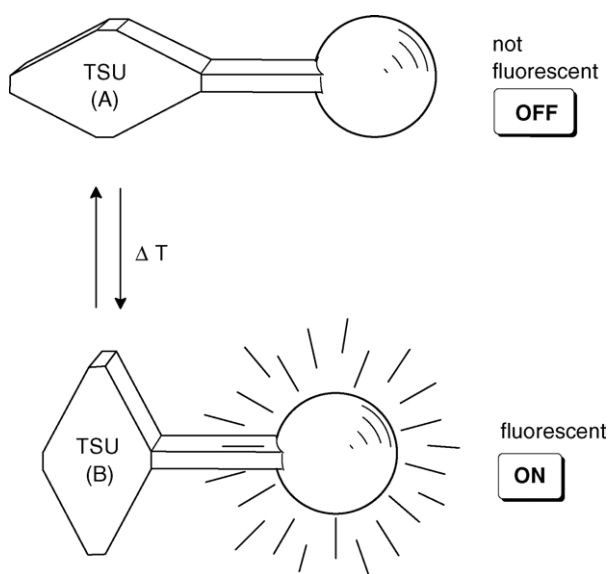

Fig. 39. The design of a molecular fluorescent thermometer. The light emission of the fluorescent fragment Fl* is controlled by the temperature sensitive unit TSU. TSU exists in two states, A and B, which have a different perturbing effect on Fl*. A and B are connected through a temperature-dependent equilibrium. Adapted from Ref. [36].

signal. In this case, the control unit should be a molecular fragment sensitive to temperature changes, which should be covalently linked to the signalling unit (see the scheme illustrated in Fig. 39). In particular, the temperature sensitive unit (TSU) should exist in two different states, A and B, connected through a fast and reversible equilibrium. Essential prerequisites are: (i) the equilibrium must be temperature-dependent,

either endothermic or exothermic; (ii) A and B must interfere with the proximate fluorescent fragment to a distinctly different extent.

Let us consider, for instance the case that: (1) the A-to-B equilibrium is endothermic, and (2) state A quenches the nearby photoactive fragment and state B does not. In such circumstances, a temperature increase will induce an increase of the concentration of A, which results in an enhancement of the fluorescence intensity. Thus, the two-component system will behave as a thermometer and the I_F versus temperature plot (which in the present case should have a positive slope) represents its calibration curve. Notice that, in principle, four types of fluorescent thermometer can be built according to (i) whether A or B exerts the perturbing effect on the fluorophore, and (ii) whether the A-to-B equilibrium is endo- or exo-thermic, as illustrated in Table 1. In two cases, the I_F versus temperature plot has a positive slope, in the other two, the slope is negative.

Notice that modes 1 and 4, which involve a positive slope of the fluorescence intensity versus temperature curve, provide the most beneficial behaviour. In fact, a temperature increase per se amplifies molecular vibrations, thus favouring the non-radiative decay of the excited fluorophore. Fluorescence enhancement with temperature contrasts the natural tendency and allows an unambiguous detection of the thermal behaviour.

A convenient TSU fragment is provided by coordination chemistry. In particular, the nickel(II) complex of the macrocyclic tetramine cyclam (3), when dissolved in a polar medium (water, MeCN) exists in two forms at the equilibrium: (a) a distorted octahedral species in which cyclam co-

Table 1
The four possible types of fluorescent molecular probes based on the design illustrated in Fig. 36

	A activity on Fl*	B activity on Fl*	Thermal nature of the A-to-B conversion	Slope of the I_F vs. temperature plot
1	Quenches	Does not quench	Endothermic	Positive
2	Quenches	Does not quench	Exothermic	Negative
3	Does not quench	Quenches	Endothermic	Negative
4	Does not quench	Quenches	Exothermic	Positive

planarly chelates the Ni^{II} centre and two solvent molecules, S, occupy the axial sites of the elongated octahedron; in the $[Ni^{II}(cyclam)S_2]^{2+}$ complex, the metal centre has two unpaired electrons and is *high-spin*; (b) a square-planar species, obtained from species (a) through the release of the two solvent molecules; in the square $[N^{II}(cyclam)]^{2+}$ complex, the stronger in-plane metal–ligand interactions induce the pairing of the two highest energy electron, to give a diamagnetic, *low-spin* species [35]. The spin interconversion equilibrium is illustrated below:

$$[Ni^{II}(cyclam)S_2]^{2+} \rightleftharpoons [Ni^{II}(cyclam)]^{2+} + 2S \qquad (1)$$
blue, high-spin, octahedral   yellow, low-spin, square-planar
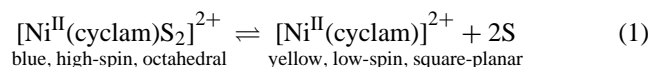
The equilibrium is reversible, fast and temperature-dependent. In particular, the (high-spin)-to-(low-spin) conversion is *endothermic*. This means that the high-spin form predominates at low temperatures, and that a temperature increase causes the concentration of the low-spin species to grow.

36
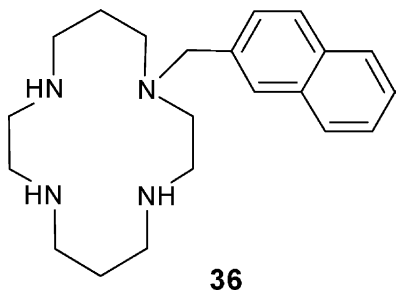
Having ascertained that the Ni^{II}/cyclam system can be a convenient TSU, the macrocycle was linked to a classic aromatic fluorophore, naphthalene, to give **36**, and the corresponding nickel(II) complexes with a variety of counterions, X^-, were prepared: Ni^{II}(**36**)X_2 [36]. In the solid state, the X^- anions occupy the axial sites of a more or less elongated octahedron and their coordinating tendencies determine the spin state of the Ni^{II} centre. When X^- is a strongly coordinating anion (Cl^-, NCS^-, NO_3^-), the complex is high-spin; when it is poorly coordinating (ClO_4^-, $CF_3SO_3^-$) the complex is low-spin. Next, the emitting behaviour of the various Ni^{II}(**36**)X_2 complex salts was investigated in a CHCl_3 solu-
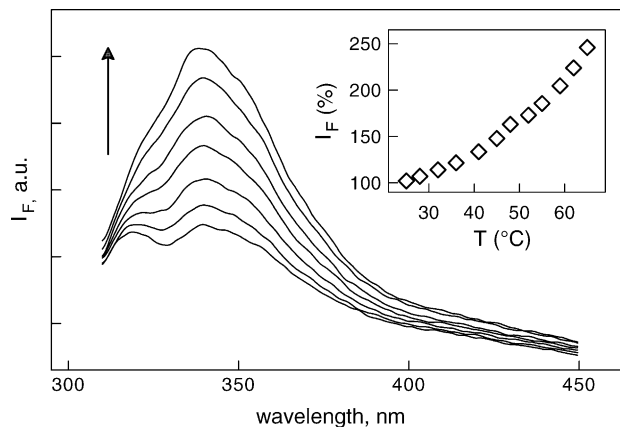

Fig. 40. The emission spectra of a 10^{-6} M solution of Ni^{II}(**36**)(CF_3SO_3)_2 in MeCN, recorded over the 27–65 °C temperature range: on increasing temperature, the fluorescence intensity, I_F, grows. The I_F vs. temperature plot (inset) provides the calibration curve of the molecular fluorescent thermometer. Adapted from Ref. [36].

tion. CHCl_3 molecules are not coordinating at all and, in CHCl_3 solution, each complex maintains the same structure and spin multiplicity as in the solid state. It was observed that in low-spin complexes the naphthalene emission was distinctly higher than for high-spin complexes (quantum yield: low-spin: $\Phi = 0.019$ for ClO_4^-, 0.020 for $CF_3SO_3^-$; high-spin: $\Phi = 0.009$ for NO_3^-, 0.005 for NCS^-, 0.007 for Cl^-). Transition metal ions like Ni^{II}, when encircled by the cyclam ring, tend to quench the *N*-linked fluorophore through an energy transfer (ET) mechanism, of the double electron exchange type. The emission behaviour of Ni^{II}(**36**)X_2 complexes in CHCl_3 indicates that this ET mechanism is more efficient with the high-spin metal centre than with the spin paired cation, which exhibits a sort of 'closed shell' electronic configuration.

Following this information, the Ni^{II}–**36** system should behave as a type (1) thermometric probe, according to the classification illustrated in Table 1. In fact, a solution of Ni^{II}(**36**)(CF_3SO_3)_2 in MeCN at room temperature is poorly fluorescent. On increasing temperature, the naphthalene emission sharply increases, as illustrated in Fig. 40. In the polar MeCN medium, the Ni^{II}(**36**)(CF_3SO_3)_2 salt disso-

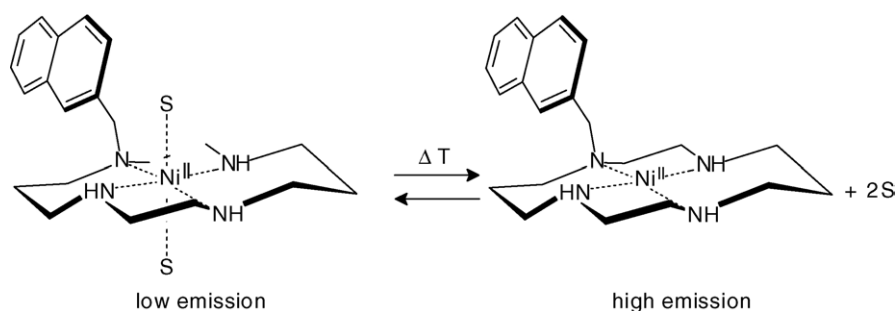low emission   high emission

Fig. 41. The high-spin to low-spin interconversion equilibrium which takes places with the Ni^{II}–**36** system in a polar solvent S. As the high- to low-spin conversion is endothermic, a temperature increase makes fluorescence increase. The two forms reversibly interconvert in less than 1 ms and the thermometric response is practically instantaneous. Adapted from Ref. [36].

ciates and the complex cation undergoes the interconversion equilibrium, involving two solvent molecules S, illustrated by Fig. 41.

At lower temperatures, the octahedral high-spin complex dominates, which has a pronounced quenching effect: fluorescence is low. On increasing temperature, the endothermic spin conversion takes place and the relative concentration of the low-spin species increases: this species exerts a much lower perturbing effect on the fluorophore, whose emission is restored.

The response of the thermometer is practically instantaneous since the change of the emission intensity, both decrease and increase, is related to extremely fast events (1) release/uptake of two solvent molecules by the labile Ni^{II} ion; (2) rearrangement of d electrons to the high-/low-spin configurations; (3) double electron exchange between the excited fluorophore and the metal centre. The three processes, on the whole, are well below the millisecond time scale.

8. Concluding remarks

All the molecular systems described in the previous sections have been synthesised and investigated in our laboratory over the past decade. Their common feature is that they result from the association, covalent or non-covalent, of a metal containing subunit and a fluorescent fragment. Such systems may exist in two different states, which are defined by the oxidation state of the metal, the position of the metal centre in a two-compartment ligand, the coordinative arrangement around the metal, etc. Each state exerts a different effect on a nearby fluorogenic fragment, giving rise to switching ON/OFF of the fluorescence. Systems which can exist in two different forms generate digital states "1" and "0" and may represent the elementary components of a computer operating on single molecule activity [37]. The use of two-state systems containing metal centres, like those described in this article, has to be explored for the application. Transition metals bring several properties which may be useful from the point of view of the design of switchable systems at the molecular level, under a variety of stimuli. These properties include, among others: (i) rich and versatile redox activity, (ii) easy and fast modification of stereochemistry and of the coordination number, (iii) variation of the magnetic features, through spin interconversion equilibria. Moreover, transition metals, depending upon their electronic configuration, are capable of selective intramolecular interactions with proximate fluorogenic fragments. Thus transition metals can be conveniently used for the design of two-state molecular devices displaying a switchable light-emitting activity. Time will reveal whether such elementary devices could form the basis of molecular computers or similar digital machines. Meanwhile, they have to be considered useful and, sometimes, amusing steps in the beneficial exercise of generating functions at the molecular level.

References

[1] A. Weller, Pure Appl. Chem. 16 (1968) 115.
[2] A. Juris, M.T. Gandolfi, M.F. Manfrin, V. Balzani, J. Am. Chem. Soc. 98 (1976) 1047.
[3] A.P. de Silva, R.A.D.D. Rupasinghe, J. Chem. Soc., Chem. Commun. (1985) 1660.
[4] V. Goulle, A. Harriman, J.-M. Lehn, J. Chem. Soc., Chem. Commun. (1993) 134.
[5] L. Fabbrizzi, M. Licchelli, P. Pallavicini, Acc. Chem. Res. 32 (1999) 846.
[6] V. Amendola, L. Fabbrizzi, C. Mangano, P. Pallavicini, Acc. Chem. Res. 34 (2001) 488.
[7] (a) L. Fabbrizzi, A. Poggi, Chem. Soc. Rev. 24 (1995) 197;
(b) A.P. de Silva, H.Q.N. Gunaratne, T. Gunnlaugsson, A.J.M. Huxley, C.P. McCoy, J.T. Rademacher, T.E. Rice, Chem. Rev. 97 (1997) 1515;
(c) V. Balzani, M. Venturi, A. Credi, Molecular Devices and Machines, Wiley–VCH, Weinheim, 2003, and references therein.
[8] R. Bergonzi, L. Fabbrizzi, M. Licchelli, C. Mangano, Coord. Chem. Rev. 170 (1998) 31.
[9] D.H. Busch, Acc. Chem. Res. 11 (1978) 392.
[10] E.J. Billo, Inorg. Chem. 23 (1984) 236.
[11] L. Fabbrizzi, Comments Inorg. Chem. 4 (1985) 33.
[12] M. Calligaris, O. Carugo, G. Crippa, G. De Santis, M. Di Casa, L. Fabbrizzi, A. Poggi, B. Seghi, Inorg. Chem. 29 (1990) 2964.
[13] L. Fabbrizzi, M. Licchelli, S. Mascheroni, A. Poggi, D. Sacchi, M. Zema, Inorg. Chem. 41 (2002) 6129.
[14] G. De Santis, L. Fabbrizzi, M. Licchelli, N. Sardone, A.H. Velders, Chem. Eur. J. 2 (1996) 1243.
[15] G. De Santis, L. Fabbrizzi, M. Licchelli, C. Mangano, D. Sacchi, Inorg. Chem. 34 (1995) 3581.
[16] M. Di Casa, L. Fabbrizzi, M. Licchelli, A. Poggi, D. Sacchi, M. Zema, J. Chem. Soc., Dalton Trans. (2001) 1671–1675.
[17] S.C. Cummings, R.E. Sievers, Inorg. Chem. 9 (1970) 1131.
[18] L. Fabbrizzi, M. Licchelli, C. Rospo, D. Sacchi, M. Zema, Inorg. Chim. Acta 300–302 (2000) 453.
[19] P. Pallavicini, A. Perotti, B. Seghi, L. Fabbrizzi, J. Am. Chem. Soc. 109 (1987) 5139.
[20] D.K. Cabbiness, D.W. Margerum, J. Am. Chem. Soc. 91 (1969) 6540.
[21] L. Fabbrizzi, M. Licchelli, P. Pallavicini, L. Parodi, Angew. Chem. Int. Ed. Engl. 37 (1998) 800.
[22] L. Fabbrizzi, F. Foti, M. Licchelli, P.M. Maccarini, D. Sacchi, M. Zema, Chem. Eur. J. 8 (2002) 4965.
[23] J.-M. Lehn, Supramolecular Chemistry, Concepts and Perspectives, VCH, Weinheim, 1995;
E.C. Constable, Angew. Chem. Int. Ed. Engl. 30 (1991) 1450.
[24] V. Amendola, L. Fabbrizzi, L. Linati, C. Mangano, P. Pallavicini, V. Pedrazzini, M. Zema, Chem. Eur. J. 5 (1999) 3679.
[25] V. Amendola, L. Fabbrizzi, L. Gianelli, C. Maggi, C. Mangano, P. Pallavicini, M. Zema, Inorg. Chem. 40 (2001) 3579.
[26] V. Amendola, L. Fabbrizzi, P. Pallavicini, E. Sartirana, A. Taglietti, Inorg. Chem. 42 (2003) 1632.
[27] V. Balzani, M. Gómez-López, J.F. Stoddart, Acc. Chem. Res. 31 (1998) 405.

[28] J.-P. Sauvage, Acc. Chem. Res. 31 (1998) 611.

[29] V. Amendola, L. Fabbrizzi, M. Licchelli, C. Mangano, P. Pallavicini, L. Parodi, A. Poggi, Coord. Chem. Rev. 190–192 (1999) 649.

[30] V. Amendola, L. Fabbrizzi, C. Mangano, P. Pallavicini, A. Perotti, A. Taglietti, J. Chem. Soc., Dalton Trans. (2000) 185.

[31] V. Amendola, L. Fabbrizzi, C. Mangano, H. Miller, P. Pallavicini, A. Perotti, A. Taglietti, Angew. Chem. Int. Ed. 41 (2002) 2553.

[32] G. De Santis, L. Fabbrizzi, M. Licchelli, A. Poggi, A. Taglietti, Angew. Chem. Int. Ed. Engl. 35 (1996) 202.

[33] I. Bruseghini, L. Fabbrizzi, M. Licchelli, A. Taglietti, Chem. Commun. (2002) 1348.

[34] M. Di Casa, L. Fabbrizzi, M. Licchelli, A. Poggi, A. Russo, A. Taglietti, Chem. Commun. (2001) 825.

[35] A. Anichini, L. Fabbrizzi, P. Paoletti, R.M. Clay, Inorg. Chim. Acta 24 (1977) L21.

[36] L. Fabbrizzi, M. Licchelli, A. Poggi, G. Rabaioli, A. Taglietti, in: B. Valeur, J.-C. Brochon (Eds.), New Trends in Fluorescence Spectroscopy. Application to Chemical and Life Sciences, Springer, Heidelberg, 2001, pp. 209–227.

[37] D. Rouvray, Chem. Br. (1998) 26–29.